Published in final edited form as:
Nat Immunol. 2021 August 01; 22(8): 1042–1051. doi:10.1038/s41590-021-00969-3.

Adenovirus vector vaccination reprograms pulmonary fibroblastic niches to support protective inflating memory CD8+ T cells

Jovana Cupovic[1,2], **Sandra S. Ring**[1], **Lucas Onder**[1], **Julia M. Colston**[3], **Mechthild Lütge**[1], **Hung-Wei Cheng**[1], **Angelina De Martin**[1], **Nicholas M. Provine**[3], **Lukas Flatz**[1,4], **Annette Oxenius**[5], **Elke Scandella**[1], **Philippe Krebs**[6], **Daniel Engeler**[7], **Paul Klenerman**[#3], **Burkhard Ludewig**[#1,8]

[1]Institute of Immunobiology, Kantonsspital St. Gallen, St. Gallen, Switzerland [2]Max Planck Institute for Immunobiology and Epigenetics, Freiburg, Germany [3]Peter Medawar Building for Pathogen Research, Nuffield Department of Medicine, University of Oxford, Oxford, United Kingdom [4]Department of Dermatology, University Hospital Zurich, Zurich, Switzerland [5]Institute of Microbiology, ETH Zurich, Zurich, Switzerland [6]Institute of Pathology, University of Berne, Berne, Switzerland [7]Department of Urology, Kantonsspital St. Gallen, St. Gallen Switzerland [8]Institute of Experimental Immunology, University of Zurich, Zurich, Switzerland

[#] These authors contributed equally to this work.

Abstract

Pathogens and vaccines that produce persisting antigens can generate expanded pools of effector memory CD8$^+$ T cells described as memory inflation. While the properties of inflating memory CD8$^+$ T cells have been characterized, the specific cell types and tissue factors responsible for their maintenance remain elusive. Here, we show that clinically applied Adenovirus vectors preferentially target fibroblastic stromal cells in cultured human tissues. Moreover, we have used cell type-specific antigen targeting to define critical cells and molecules that sustain long-term antigen presentation and T cell activity after Adenovirus vector immunization in mice. While antigen targeting to myeloid cells was insufficient to activate antigen-specific CD8$^+$ T cells, genetic activation of antigen expression in Ccl19-Cre-expressing fibroblastic stromal cells induced inflating CD8$^+$ T cells. Local ablation of vector-targeted cells revealed that lung fibroblasts

Correspondence to: Paul Klenerman; Burkhard Ludewig.

Lead contact/corresponding authors: Burkhard Ludewig, burkhard.ludewig@kssg.ch and Paul Klenerman, paul.klenerman@medawar.ox.ac.uk.

Author contributions statement
B.L., P.Kl. and J.C. designed the study, discussed data and wrote the paper. J.C., J.M.C, S.S.R., L.O., A.D.M., H.-W.C., D.E. conducted experiments and discussed data. M.L. performed bioinformatics analyses and discussed data. N.P. discussed data and provided reagents. P.Kr. and A.O. discussed data and provided reagents. L.F. and E.S. discussed data.

Competing interests statement
L.F. is a co-founder and shareholder of Hookipa Pharma Inc. B.L., L.O. and H.-W.C. are co-founders and shareholders of Stromal Therapeutics AG. S.R. and H.-W.C. are part-time employees of Stromal Therapeutics AG. The remaining authors declare no competing interests.

Europe PMC Funders Author Manuscripts

support protective support protective function and metabolic fitness inflating memory T cells in an IL-33-dependent manner. Collectively, these data define a critical fibroblastic niche that underpins robust protective immunity operating in a clinically important vaccine platform.

Introduction

The ultimate goal of T cell-based vaccination strategies is the induction of long-term immunological protection via effector memory T cells [1]. Adenovirus (Ad) vector-based vaccines using the backbone of human Ads have been shown in clinical studies to be highly immunogenic with induction of specific antibody and/or T cell responses against viral [2, 3] or cancer antigens [4]. However, pre-existing anti-Ad antibodies in vaccinated individuals reduce immunogenicity and efficacy of vaccines based on human Ads [2, 4], which led to the development of non-human vectors based on chimpanzee viruses [5]. Chimeric Ad vectors have been shown to induce long-lived T cell responses against SARS-CoV-2 [6, 7] and to generate polyfunctional central and effector memory T cells against hepatitis C virus [8]. Other approaches to circumvent preexisting anti-Ad vector immunity include the utilization of viral backbones with rare serotypes such as Ad26 [3] or prime-boost regimen with rAd26-S given on day 0 and rAd5-S on day 21 [9]. Although the clinical development of Ad-based vaccines is well-advanced, the basic features that determine the high immunogenicity of these viral vectors are still largely unclear.

One of the prominent qualities of Ad vectors that can guide their further improvement is the generation of inflating memory $CD8^+$ T cells [10]. Steadily growing memory $CD8^+$ T cell pools have been initially described for the murine cytomegalovirus (MCMV) infection [11, 12, 13]; a feature that is most likely associated with the continued generation of antigenic peptides during viral reactivation in peripheral tissues [14]. The persistent expansion of effector memory T cell populations (i.e. “high” for CX3CR1, KLRG1, and “low” for CCL7, CD62L, CD28, CD27, CD127) occurs not only during MCMV infection [15], but is one of the hallmarks of an inflationary $CD8^+$ T cell response against human CMV [16, 17]. Utilization of replication-defective, recombinant Ad5-based vectors has further guided the molecular characterization of inflationary $CD8^+$ T cell memory. Immunization with beta-galactosidase (bgal)-expressing Ad results in long-lasting transduction of cells in peripheral organs such as liver and lung, leading to the generation of antigenic peptides for several months [18]. The bgal-transgene harbors two H2-K^b-restricted antigenic peptides; one epitope generating an expanding-contracting central-memory $CD8^+$ T cell pool and the second epitope producing an inflating effector-memory T cell response [18, 19]. The continuously expanding $CD8^+$ T cell population depends on the presence of MHCII-positive cells, while antigen-processing in professional antigen-presenting cells seems to be dispensable [18]. Thus, it appears that antigen presentation by non-hematopoietic cells is crucial for the generation of inflating memory $CD8^+$ T cell responses following Ad-vector immunization [18, 20]. However, the nature of such long-lived, non-hematopoietic cells has remained elusive.

Lymphoid organ stromal cells, i.e. lymphatic and blood endothelial cells and fibroblastic reticular cells, generate not only the infrastructure for lymphocyte entry and exit, but provide dedicated niches for lymphocyte activation, differentiation and maintenance [21, 22, 23]. During

Europe PMC Funders Author Manuscripts

MCMV infection, it is assumed that antigen-presenting stromal cells drive memory inflation through the interaction with cross-presenting dendritic cells in lymphoid organs [24, 25, 26]. In addition, stromal cells can provide key growth factors, such as IL-15, for the long-term sustenance of inflating memory T cells [27]. Here, we describe that clinically relevant Ad vaccine vectors target preferentially fibroblastic stromal cells (FSCs) in explant cultures of human tonsillar tissue. The target cell selectivity of HuAd5-based vectors for podoplanin (PDPN)-expressing FSCs was confirmed in murine models that restrict Ad vector-mediated transgene expression to Cre recombinase-positive cells. We found that long-term transduction of Ccl19-Cre$^+$ FSCs in the lung was crucial for the induction and sustenance of inflating memory CD8$^+$ T cells, which can protect the host from metastasizing cancer. Importantly, adenovirus-based vaccination induced reprogramming of pulmonary FSCs that fostered the generation of a distinct IL-33-producing FSC subset. In sum, adenoviral vectors transform the pulmonary fibroblastic landscape and thereby generate microenvironmental niches that are crucial for the maintenance of protective inflationary memory CD8$^+$ T cells.

Results

Targeting of human fibroblasts by Ad vectors

Human Ads were first described as cytopathogenic agents isolated from human adenoid tonsils [28]. Here, we used sliced tissue cultures from human palatine tonsils to assess the cellular tropism of green fluorescent protein (GFP)-expressing Ad vectors (Extended Data Fig. 1a). Both HuAd5-GFP and ChAdOx1-GFP vectors readily transduced cells in the tissue slides with PDPN$^+$ CD45$^-$ cells most frequently expressing the GFP transgene (Fig. 1a and b). Next, we compared side-by-side the susceptibility to infection with the recombinant Ad vectors of short-term cultured tonsillar stromal cells (TSCs) and peripheral blood mononuclear cells (PBMCs). Both ChAdOx1-GFP (Fig. 1c and d) and HuAd5-GFP (Fig. 1e and f) efficiently transduced TSCs following an incubation of 3 h, while the transduction rate of PBMCs remained low. Even at a high multiplicity of infection (MOI) of 1,000 particles per cells, less than 2% of the hematopoietic cells were GFP-positive (Fig. 1d and f). Those hematopoietic cells that expressed the viral transgene were mainly CD14$^+$ HLA-DR$^+$ monocytes (Extended Data Fig. 1b to d). The majority of GFP$^+$ cells in cultured TSCs were PDPN$^+$ fibroblasts with only few CD31$^+$ endothelial cells harboring the transgene following exposure to ChAdOx1-GFP (Extended Data Fig. 1e and 1f) or HuAd5-GFP (Extended Data Fig. 1e and 1g). In addition, both ChAdOx1 and HuAd5 vectors delivered the transgene to PDPN$^+$ fibroblasts in cultured human skin stromal cell (Extended Data Fig.1 h-j) and cultured lung stromal cell preparations (Extended Data Fig.1 k-m). These data demonstrate that clinically relevant Ad vectors efficiently transduce human fibroblasts derived from both lymphoid and non-lymphoid organs.

FSC-dependent induction of inflating memory CD8$^+$ T cells

HuAd5-based vectors expressing the bgal antigen elicit inflating memory CD8$^+$ T cell responses in mice with up to 30% of CD8$^+$ T cells in peripheral blood and up to 40% of CD8$^+$ T cells in lung recognizing the bgal$_{96}$ epitope, while the bgal$_{497}$ epitope generates a classical contracted memory CD8$^+$ T cell population ((Extended Data Fig. 2a-d) and [18]). To restrict transgene expression to specific cell types in mice, we engineered a cassette with

double-floxed Cre recombinase recognition sites in inverted orientation flanking the LacZ gene [29] and generated a HuAd5-based vector termed Ad-LacZ/FlexON (Fig. 2a). Injection of Ad-LacZ/FlexON into mice with ubiquitous Cre recombinase expression led to the inflation of bgal$_{96}$ epitope-specific CD8$^+$ T cells (Extended Data Fig. 2e). To probe the ability of different myeloid cell populations to induce and expand inflating memory CD8$^+$ T cell pools in response to Ad vector vaccination, we immunized Cd11c-Cre and LysM-Cre mice with Ad-LacZ/FlexON. We found that the frequency of bgal$_{96}$-specific CD8$^+$ T cells in mice with Cre recombinase expression in CD11c$^+$ dendritic cells (Fig. 2b, c) or LysM$^+$ macrophages/neutrophils (Extended Data Fig. 2 f, g) was not substantially elevated compared with Cre-negative control mice. In stark contrast, mice with Cre recombinase expression in Ccl19-Cre$^+$ fibroblastic reticular cells in lymphoid organs [30, 31] and dedicated niches in peripheral organs [32, 33] showed pronounced expansion of bgal$_{96}$ epitope-specific CD8$^+$ T cells (Fig. 2d, e). Neither Cd11c-Cre nor LysM-Cre mice showed substantial activation of bgal$_{497}$-specific CD8$^+$ T cells (Fig. 2 f, g and Extended Data Fig. 2g), whereas expanding-contracting CD8$^+$ T cell pools reactive to the bgal$_{497}$ epitope were induced in Ccl19-Cre mice (Fig. 2 h and i). Collectively, our findings reveal that Ad vectors efficiently target FSCs and that particular FSC populations – highlighted by the Ccl19-Cre transgene in mice – are crucial for the induction of memory CD8$^+$ T cell inflation.

FSC-DC cooperation supports inflating memory CD8$^+$ T cells

Next, we investigated whether Ccl19-Cre$^+$ cells are sufficient to induce inflating memory CD8$^+$ T cells after Ad vector immunization. In a first set of experiments, we restricted the peptide presentation capacity to non-hematopoietic cells through the transfer of H2-K^b-deficient bone marrow into sub-lethally irradiated Ccl19-Cre mice (Fig. 3 a). We found that control mice with MHCI-competent bone marrow cells generated inflating bgal$_{96}$-specific CD8$^+$ memory T cells (Fig. 3b and c) in magnitude and kinetics that were comparable with non-irradiated Ccl19-Cre mice (Fig. 2e and Extended Data Fig. 2a-c). In contrast, memory inflation of bgal$_{96}$-specific CD8$^+$ T cells was almost completely blocked in Ccl19-Cre mice harboring H2-K^b-deficient hematopoietic cells (Fig. 3b and c). Likewise, bone marrow chimeric Ccl19-Cre mice with a deficiency in cross-presenting dendritic cells due to the lack of basic leucine zipper ATF-Like transcription factor 3 (*Batf3*) [34] in their hematopoietic compartment (Fig. 3d), failed to generate inflating bgal$_{96}$-specific CD8$^+$ memory T cells (Fig. 3e and f). The impaired cross-presentation due to the absence H2-K^b (Extended Data Fig. 3a) or *Batf3* expression (Extended Data Fig. 3b) in the hematopoietic compartment of bone marrow chimeric Ccl19-Cre mice almost completely abolished the expansion of bgal$_{497}$-specific CD8$^+$ T cells. These results indicate that Ccl19-Cre$^+$ FSCs require the cooperation with MHC class I-competent, cross-presenting dendritic cells to facilitate priming and expansion of inflationary memory CD8$^+$ T cells after immunization with bgal-recombinant Ad vectors.

Pulmonary Ccl19-Cre$^+$ FSCs support inflationary CD8$^+$ T cells

Following intravenous application, the Ad-LacZ vector transduces target cells mainly in liver, lung, and spleen [18, 35]. Since Ad-LacZ/FlexON vaccination of splenectomized Ccl19-Cre mice did not significantly alter the inflationary CD8$^+$ cell response against the bgal$_{96}$ epitope (Extended Data Fig. 4a), we concluded that FSCs mediating memory inflation most

likely reside in non-lymphoid organs. To assess to what extent Ccl19-Cre$^+$ FSCs in the lung affect memory inflation, we utilized an organ-specific cell ablation protocol in Ccl19-EYFP/iDTR mice 33, which highlight Ccl19-Cre lineage-positive cells with the fluorescent marker EYFP and facilitate ablation of genetically tagged cells by intranasal application of diphtheria toxin (DT) (Extended Data Fig. 4b and c). Ccl19-Cre$^+$ FSCs in lung tissue include smooth muscle actin (ACTA2)-positive vascular smooth muscle/adventitial cells (Fig. 4a). Intranasal DT application significantly reduced the number of EYFP$^+$ cells in the lung (Fig. 4a and Extended Data Fig. 4c), whereas transgene expression in other organs such as the mediastinal lymph node (Fig. 4a), liver and spleen (Extended Data Fig. 4d) was not affected. In contrast, systemic DT application via intraperitoneal injection led to almost complete ablation of Ccl19-Cre$^+$ FSCs cells in lung, mediastinal lymph node (Fig. 4a), liver and spleen (Extended Data Fig. 4d). As described previously [36], ablation of Ccl19-Cre$^+$ cells in lymph nodes following systemic DT application precipitated impaired immune cell organization and cellularity (Fig. 4a). Consequently, systemic ablation of Ccl19-Cre$^+$ FSCs in Ccl19-EYFP/iDTR mice led to a significantly reduced expansion of bgal$_{96}$-specific CD8$^+$ T cells in blood and lung on day 21 when compared to PBS-treated controls (Fig. 4b and Extended Data Fig. 4e). Likewise, the local depletion of EYFP$^+$ FSCs in the lung through i.n. DT application reduced CD8$^+$ T cells inflation in blood and lung (Fig. 4b and Extended Data Fig. 4e), suggesting that Ccl19-Cre$^+$ FSCs in the lung are the major cell population that drives the activation of inflating bgal$_{96}$-specific CD8$^+$ T cells. The effect of local, lung-restricted depletion of EYFP$^+$ FSCs on expansion of inflating bgal$_{96}$-specific CD8$^+$ T cells became evident early after T cell activation (day 14) and was maintained until day 50 after immunization (Fig. 4c). The frequencies of bgal$_{497}$-specific CD8$^+$ T cells were not substantially altered by either of the ablation protocols (Extended Data Fig. 4f and g). CD8$^+$ T cells in the lungs accumulated in the vicinity of pulmonary blood vessels with single CD8$^+$ T cells being in close contact with EYFP$^+$ FSCs in Ad-LacZ/FlexON vaccinated Ccl19-EYFP/iDTR mice treated with PBS on day 21 (Fig. 4d, arrowheads). Such cellular aggregations harbored lymphocytes and macrophages leading to a significant increase of immune cell content compared to naive Ccl19-EYFP/iDTR mice (Fig. 4e). Intranasal DT treatment reduced immune cell accumulation in lungs of Ccl19-EYFP/iDTR mice with the most pronounced effect on CD8$^+$ T cells (Fig. 4e and Extended data Fig. 4h). To assess whether ablation of Ccl19-Cre$^+$ FSCs in lungs affects the protective capacity of pulmonary immune cells, we challenged DT- or PBS-treated Ccl19-EYFP/iDTR mice with bgal-expressing melanoma cells on day 21 after Ad-LacZ/FlexON immunization (Fig. 4f). Mice with an intact lung FSC infrastructure controlled the metastatic growth of the tumor cells, whereas DT-treated mice were not protected and showed significantly higher presence of tumor nodules in the lung (Fig. 4 g and h). In sum, these data demonstrate that Ccl19-Cre$^+$ FSCs not only substantially contribute to the expansion of inflationary memory CD8$^+$ T cells that protect the host from metastasizing tumor, but also transform the immune cell landscape in the lung in long-term.

Adenovirus vectors reprogram Ccl19-Cre$^+$ lung fibroblasts

Although the number of Ccl19-Cre$^+$ lung FSCs – highlighted by EYFP expression in Ccl19-Cre R26R-EYFP (Ccl19-EYFP) mice – was not increased on day 21 post Ad-LacZ/FlexON immunization (Fig. 5a and Extended Data Fig. 5a), the cells showed a distinct activation

pattern with enhanced surface expression of PDPN (Fig. 5b and Extended Data Fig. 5b), the adhesion molecule ICAM1 (Fig. 5c and Extended Data Fig. 5c), and platelet-derived growth factor receptor-alpha (PDGFRα, CD140a) (Fig. 5d and Extended Data Fig. 5d). The expression of other canonical FSC markers such as PDGFRβ (Extended Data Fig. 5e) or the adhesion molecule VCAM1 (Extended Data Fig. 5f) was not substantially affected by the Ad-LacZ/FlexON immunization. To elaborate in more detail the molecular changes induced by the viral vector in pulmonary Ccl19-Cre^{+} cells, we took advantage of the EYFP expression in Ccl19-EYFP mice to enrich the cells and to analyze the transcriptome from naive and Ad-LacZ/FlexON-immunized mice by single-cell RNA sequencing (scRNA-seq). Unsupervised clustering of the combined samples defined six conserved clusters visualized with uniform manifold approximation and projection (UMAP; Fig. 5e, f). Computation of cluster-specific genes combined with the analysis of known lung fibroblast signatures [37, 38, 39] revealed transcriptional signatures consistent with two clusters of pulmonary fibroblasts (designated as *Aqup1* ^{high} and *Npnt* ^{high}) (Extended Data Fig. 6a), which form major fractions of EYFP^{+} cells from both naive and immunized lungs (Fig. 5f). Vascular smooth muscle cells (SMCs), characterized by the expression of *Acta2*, *Tagln* and *Myh11*, could be distinguished from pericytes (PCs), which are marked by the expression of *Cox4i2*, *Postn* and *Notch3* (Extended Data Fig. 6a). The molecular signature of the third steady-state fibroblast fraction was distinguished by high-level expression of *Lum* (Fig. 5f and Extended Data Fig. 6a). Adenovirus immunization induced the appearance of a molecularly distinct fraction with high expression of the cytokine *Il33* (Fig. 5e-f and Extended Data Fig. 6a). *Il33* ^{high} fibroblasts appeared to be related to *Lum* ^{high} fibroblasts as revealed by cluster similarity analysis (Fig. 5g). Using RNA velocity analysis of single cells, which provides a predictive value for cellular state progression based on the balance between unspliced and spliced mRNAs [40], we found that Ad vector immunization induced dynamic changes in the SMC and PC compartments (Extended Data Fig. 6c). Likewise, the *Il33* ^{high} cell fraction showed highly dynamic gene expression suggesting ongoing differentiation processes, while the related *Lum* ^{high} population was rather static (Extended Data Fig. 6c). Differential gene expression analysis between the two cell fractions showed that the *Il33* ^{high} fibroblast population exhibits more immune-stimulatory functions with upregulation of *Il33* and *Ly6a* expression (Fig. 5h and i) and suggested that the Ad immunization transforms the *Lum* ^{high} population from a structural, extracellular matrix-producing population to a metabolically active and immune -stimulating cell fraction (Extended Data Fig. 6b). This interpretation was supported by flow cytometric validation of the increased abundance of stem cell antigen-1 (Sca-1, encoded by the *Ly6a* gene)/CD34-expressing EYFP^{+} fibroblasts (Extended Data Fig. 6 d, e) and by RT-PCR analysis showing increased expression of *Il33* in EYFP^{+} lung cells of Ad vaccinated compared to naive mice (Extended Data Fig. 6f). Moreover, the Sca-1^{+}/CD34^{+} fraction of EYFP-expressing cells in lungs of Ad vaccinated mice showed increased expression of *Il33* mRNA compared to EYFP^{+} Sca-1^{-} cells (Extended Data Fig. 6g). The elevated expression of LacZ mRNA in the Sca-1^{+}/CD34^{+} fraction of EYFP-expressing cells suggests that differentiation of *Lum* ^{high} cells into immune-stimulatory FSCs is driven – at least partially – by the persistence Ad vector-delivered antigen in these cells (Extended Data Fig. 6h). Confocal microscopy analysis of thick lung sections revealed that EYFP^{+} cells underpin mainly perivascular and peribronchial areas and that Ad vector immunization is associated with the formation of pronounced bronchus-associated lymphoid

tissues (BALT) (Extended Data Fig. 7). We found aggregations of $CD8^+$ T cells enmeshed in a reticular network of IL-33^+ $EYFP^+$ FSCs on day 21 after Ad immunization (Fig. 5j and Extended Data Fig. 6i). By day 50 post immunization, Ccl19-Cre^+ FSC-underpinned, highly organized BALT structures had developed, forming clearly distinguished areas of $B220^+$ B cells surrounded by $CD8^+$ T cells (Fig. 5j and Extended Data Fig. 6i). Overall, these results show that adenovirus immunization induces phenotypic and functional reprogramming of a distinct subset of lung fibroblasts, leading to elaboration of immune dedicated niches that support maintenance of memory $CD8^+$ T cells in the lung.

Ccl19-Cre^+ FSCs maintain inflationary $CD8^+$ T cell fitness

To further elaborate how and to what extent local immune cell-nurturing fibroblastic niches support the maintenance and function of inflating memory $CD8^+$ T cells, we used unbiased single cell transcriptomics to gauge the phenotype of $bgal_{96}$-specific $CD8^+$ T cells from the lungs of Ad-LacZ/FlexON immunized Ccl19-EYFP/iDTR mice. We found that the absence of Ccl19-Cre^+ FSCs in DT-treated mice substantially changed the transcriptome of the majority of $bgal_{96}$-specific $CD8^+$ T cells on day 21 in DT-treated mice compared with PBS-treated controls (Fig. 6a). Gene set enrichment and pathway analyses revealed that $bgal_{96}$-specifc $CD8^+$ T cells from the lungs of DT-treated mice switched to different metabolic circuits when Ccl19-Cre^+ FSC were absent. The presence of Ccl19-Cre^+ FSCs in lungs of Ad-LacZ/FlexON immunized (PBS-treated) mice led to the preservation of processes involved in the regulation of mitochondrial protein complexes including the electron transport chain and mitochondrial import, chromatin remodelers and the regulation of organelle membranes including endoplasmic reticulum-related trafficking (Fig. 6b and Extended Data Fig. 8a). In contrast, $bgal_{96}$-specific $CD8^+$ T cells deprived of Ccl19-Cre^+ FSC niches in the lung activated metabolic processes involved in the regulation of ribosome activity and mitochondrial ATP-synthase activity (Fig. 6b and Extended Data Fig. 8a). More detailed analysis of differentially expressed genes confirmed the decreased expression of genes involved in mitochondrial energy metabolism (e.g. *Cox5a*, *Cox8a*, *Ndufab1, Tomm20*) in $bgal_{96}$-specific $CD8^+$ T cells from the DT-treated group (Fig. 6c and Extended Data Fig. 8b). Memory $CD8^+$ T cells exhibit an increased mitochondrial mass that allows for improved energy provision via oxidative phosphorylation, which is required to maintain the functionality and survival of an antigen experienced T cell population [41, 42]. Although proliferation (Extended Data Fig. 8c) and survival (Extended Data Fig. 8d) were not affected by the depletion of Ccl19-Cre^+ FSCs, the analysis of the mitochondrial content of $bgal_{96}$-specific $CD8^+$ T cells isolated from DT-treated Ccl19-EYFP/iDTR mice revealed significantly lower mitochondrial mass (Fig. 6d) and mitochondrial membrane potential (Fig. 6e) compared to PBS-treated mice.

The appearance of an *Il33* ^{high} FSC population in the lung following adenovirus immunization (Fig. 5) stimulated us to cross *Il33* $^{fl/fl}$ mice with Ccl19-Cre mice. We found that the effect of cell type-specific ablation of *Il33* gene expression on the mitochondrial phenotype of $bgal_{96}$-specific $CD8^+$ T cells was similar to that of DT-treated Ccl19-EYFP/iDTR mice. Namely, mitochondrial mass (Fig. 6f, g), mitochondrial membrane potential (Fig. 6h) and the expression of mRNAs coding for elements of electron transport chain *Uqcrc2* (Cytochrome b-c1 complex subunit 2), *Sdha* (Succinate dehydrogenase complex,

subunit A) and *Cox 4I1* (Cytochrome c oxidase subunit 4 isoform 1) were significantly lower in Ccl19-Cre *Il33*$^{fl/fl}$ mice compared to Ccl19-Cre *Il33*$^{+/+}$ mice (Extended Data Fig. 8e). Moreover, *Il33* gene deficiency in Ccl19-Cre^{+} cells resulted in impaired expansion of bgal$_{96}$-specific CD8^{+} T cells on day 21 post immunization with Ad-LacZ/FlexON (Fig. 6i and Extended Data Fig. 9a). Of note, *Il33*-deficiency in Ccl19-Cre^{+} cells and local DT-mediated ablation of Ccl19-Cre^{+} lung FSCs impaired memory CD8^{+} T cell expansion to a similar degree (Fig. 6i and Extended Data Fig. 9a). Moreover, differentiation towards the effector memory phenotype with high expression of the markers KLRG1 and CX3CR1 (Fig. 6j) and the production of T cell effector cytokines (Fig. 6k and l) were affected to a similar extent by the *Il33*-deficiency and the Ccl19-Cre^{+} lung FSC ablation. The expansion of bgal$_{497}$-specific cells (Extended Data Fig. 9b), their differentiation (Extended Data Fig. 9c), and the production of T cell effector cytokines (Extended Data Fig. 9d) on day 21 after Ad-LacZ/FlexON immunization was not affected by local Ccl19-Cre^{+} FSC ablation or cell type-specific ablation of *Il33* gene expression. In sum, these data reveal that IL-33 produced by Ccl19-Cre^{+} FSCs plays a dominant role in generating pulmonary fibroblastic niches that are critical for the maintenance of the function and metabolic fitness of inflating memory CD8^{+} T cells.

Discussion

Ad vectors are a versatile vaccine platform as shown by the rapid development and clinical implementation of various formulations during the recent Sars-CoV-2 pandemic [3, 6, 9, 43, 44]. One of the prominent characteristics of Ad vectors, which is likely important for the generation of efficient cellular immune responses, is the persistence of the delivered antigen. In this study, we show that human Ad5-based vectors delivered via the intravenous route target lung FSCs and generate antigen depots in these long-lived cells. This feature is shown through a genetic approach that restricts antigen expression to specific cell types. The combination of limited antigen expression in Ccl19-Cre-positive FSCs with impaired cross-presentation in bone marrow chimeric mice demonstrates that transfer of antigen to dendritic cells is required for priming and the subsequent expansion of inflating memory CD8^{+} T cells pools. In addition, the persistence of Ad vectors in the lung tissue precipitated a profound remodeling of the FSC landscape that was associated with immune cell retention and the establishment of immune cell clusters mainly in perivascular and peribronchial niches.

Sustained antigen presentation in the local target tissue within the critical fibroblastic niche explains many of the known distinctive traits of CD8^{+} T cell responses generated by Ad vectors that underpin the high protective capacity of this vaccine platform. The phenotypic and functional traits of these cells, including the transcriptional profile, are well reproduced in human studies of CMV and importantly of adenoviral vector immunization – including chimpanzee-derived vectors as used in Covid-19 [6, 45, 46]. However, there are more features to explain. Our data provide evidence that local provision of IL-33 by Ccl19-Cre^{+} FSCs in the lung is critical for the inflationary expansion of memory CD8^{+} T cells and their function. Due to rapid conformational changes induced by the binding to its receptor, IL-33 has only a short range of action [47]. Hence, it is likely that the effect of IL-33 generated by Ccl19-Cre^{+} FSCs is limited to the tissue and the particular microenvironmental niche where the alarmin is produced. IL-33 can activate multiple cell types expressing the IL-33 receptor (ST2,

IL1RL1), including stromal niche cells to produce cytokines supporting immune cell expansion [48], and DC to mature and cross-present antigen [49]. It is thus conceivable that FSC-derived IL-33 stimulates both cross-presenting DCs and antigen-specific $CD8^+$ T cells in the particular niche environment. Indeed, IL-33 can directly stimulate T cells during acute viral infection [50], for the efficient generation of a memory/recall response [51]. Of note, provision of exogenous IL-33 has been shown to augment inflating memory $CD8^+$ T cell responses during MCMV infection, whereas the T cell priming phase was not dependent on the adjuvant effect of the cytokine [52]. It is possible that the adjuvant effect of IL-33 on inflating memory $CD8^+$ T cells depends – to some extent – on metabolic pathways that support the acquisition of an optimal energetic state and thereby fosters the survival in the peripheral tissue. Based on our data it is conceivable that IL-33 promotes mitochondrial function by increasing mitochondrial mass and membrane polarization. It will be important in future studies to determine whether inflationary memory $CD8^+$ T cells are the major – or even exclusive – target cell of IL-33 in immunostimulatory niches generated by Ad vector vaccination and whether modulation of metabolic pathways could further sustain the fitness of memory T cells in the particular tissue context.

Immunostimulatory FSCs of secondary lymphoid organs, known as fibroblastic reticular cells (FRCs), generate distinct niches for immune cell activation, differentiation and sustenance [21, 22]. For example, lymph node FRC subsets underpinning the B cell area, i.e. CXCL13-expressing follicular dendritic cells (FDC) regulate the germinal center reaction [53], while marginal reticular cells (MRC) provide niches for $CD169^+$ sinusoidal macrophages through the provision of the cytokine RANKL 54. Although the lung is not a dedicated lymphoid organ, particular areas in the lung can develop features of lymphoid organs that are described as inducible BALT [55]. The pulmonary immune cell aggregations induced by intravenous Ad vector immunization were mainly located in the vicinity of mid-sized ACTA2-positive blood vessels in the peribronchial interstitium of the hilus region. Since both LacZ DNA and mRNA can be detected for more than 100 days after Ad5-LacZ immunization [18], it is likely that Ad vector particles injected into the venous blood stream are filtered out in the vascular system of the lung leading to transduction of FSCs in the perivascular space. Moreover, it is possible that the persistence of the Ad vectors in lung FSCs provides both innate activation signals and mediates the antigen-dependent contact with lymphocytes leading to the formation of FSC-immune cell aggregates in the perivascular/peribronchial space.

The perivascular fibroblast compartment in the lung has been shown to support $CD8^+$ T cell activity against tumor cells 33 and to regulate the activity of type 2 innate lymphoid cells [56]. Molofsky and colleagues [56] have demonstrated that such adventitial niches formed by IL-33-producing fibroblasts exist in several tissues and that these circuits are important for the long-term control of helminth infection. Hence, immunostimulatory FSCs contribute to the formation of critical perivascular niches in different tissues to maintain protective T cell responses.

In sum, the approach of Ad vector-mediated generation of local antigenic depots as we have demonstrated can generate very substantial local immunity in the lung. Creating such depots in long-lived fibroblasts together with the reprogramming of fibroblastic niches to sustain

local T cell responses could be relevant in development of local immunity. Moreover, such local immune-stimulatory niches could contribute to systemic protection as evidenced by the widespread distribution of T cells following adenovirus-vectored vaccination. In the context of global pandemic infections, it is of clear relevance to further explore and potentially exploit the ability of Ad vectors and other vaccine platforms to specifically reprogram FSCs in different tissues. Research on this particular pathway for immunization against emerging pathogens in both pre-clinical models and in clinical studies could help to further accelerate vaccine development.

Methods

Mice

BAC-transgenic C57BL/6N-Tg(Ccl19-Cre)489Biat (Ccl19-Cre) mice have been previously described [30]. C57BL/6N (B6), C57BL/6N, R26R-enhanced yellow fluorescent protein (EYFP; B6.129X1-Gt[ROSA]26Sortm1[EYFP]Cos/J) mice were purchased from Charles River and LysM-Cre mice were purchased from Jackson Laboratory. *H2-K$^{b\,-/-}$* mice were purchased from Taconic Farms. R26R-iDTR (C57BL/6-Gt[ROSA]26Sortm1 [HBEGF]Awai/J) were obtained from A. Waisman (University of Mainz, Germany), and Cd11c-Cre mice were obtained from B. Reizis (New York University School of Medicine, USA) and Ubi-Cre ERT2 mice were obtained from T Vincent (Kennedy Institute, University of Oxford). The *Il33* targeting vector to generate the *Il33*$^{fl/fl}$ mice was generated by the trans-NIH Knock-Out Mouse Project (KOMP Project ID CSD88909) and obtained from the KOMP Repository (www.komp.org). To ablate *Il33* expression in a distinct FSC subset, Ccl19-Cre mice were crossed with *Il33*$^{fl/fl}$ mice. Ccl19-Cre mice were bred to R26R-EYFP or Rosa26R-iDTR and R26R-EYFP mice to generate heterozygous Ccl19-Cre R26R-EYFP and Ccl19-Cre R26R -EYFP/iDTR mice. *Batf3*$^{-/-}$ mice were obtained from M Kopf (ETH Zurich, Switzerland). All mice were housed in the Institute of Immunobiology, Kantonsspital St. Gallen under specific-pathogen-free (SPF) conditions at 22 °C and 30–70% humidity in a 12/12h light/dark cycle and provided ad libitum access to food and water. All experiments have been performed with 7 to 10 weeks old mice (males and females) in accordance with federal and cantonal guidelines (Tierschutzgesetz) under permission numbers SG08/17, SG01/18, SG07/19, SG04/20 and SG01/20 following review and approval by the respective Cantonal Veterinary Offices (St. Gallen, Switzerland).

Generation of bone marrow chimeric mice

Recipient mice were lethally irradiated with 9 Gy from a linear accelerator (Clinic of Radio-Oncology, Kantonal Hospital, St. Gallen). Within 24 h recipients were injected with 1.5–3 × 10^7 donor BM cells obtained from C57BL/6N, *H2-K$^{b-/-}$* or *Batf3*$^{-/-}$ mice. Mice were maintained on antibiotic water containing sulfadoxin and trimethoprim (Borgal; Veterinaria) for 3 weeks. From 6 weeks after BM transplantation, chimeric mice have been bled every week to assess the repopulations of the hematopoietic compartment in blood. Once full hematopoietic compartment repopulation had been achieved (8-12 weeks after BM transplantation) mice have been used in the experiments.

Cell ablation

Local lung FSC ablation was achieved by intranasally applying diphtheria toxin (DT; 8 ng in 10 μl PBS) to Ccl19-Cre R26R-EYFP/iDTR or Ccl19-Cre R26R-EYFP control mice on days 3, 5 (and 7 for tumor protection experiments) after immunization with Ad-LacZ/FlexON. Flow cytometry was used to assess ablation efficiency and lung draining lymph nodes were inspected for the integrity of the FRC network by confocal microscopy on day 7 post immunization. Systemic FSC ablation was achieved by giving intraperitoneal injection of DT (8 ng per gram body weight) [36]. Ablation efficiency was assessed by using confocal microscopy and flow cytometry.

Generation of adenoviral vectors

Ad-LacZ/FlexON vector was generated by Vector BIOLABS. The vector is based on a viral backbone of human Ad5 sequence that includes 5′ L-ITR and packaging signal. This is followed by a Flex switch that utilizes the CMV promotor and carries the LacZ gene in inverted orientation followed by a polyA tail. The 3′ end of the construct is composed of human Ad5 sequences that carry deletions in E1 and E3 genes and ends with a 3′ R-ITR. The Flex switch [29] uses two pairs of heterotypic, antiparallel loxP-type recombination sites, which first undergo an inversion of the coding sequence, followed by excision of two sites, leading to one of each orthogonal recombination site oppositely oriented and incapable of further recombination. Recombinant adenovirus expressing the bgal protein under the control of the HCMV promoter (Ad-LacZ) and lacking E1 and E3 genes was used as described previously [18]. Both vector preparations were applied intravenously (i.v.) at 1×10^8 IU/mouse (all diluted into PBS in a volume of 200 μL per mouse). Human AdHu5-GFP and chimpanzee ChAdOx1-GFP vectors were produced by the Jenner Institute Viral Vector Core Facility at the University of Oxford, UK as previously described [57].

Isolation of murine cells

Mice were sacrificed at the indicated time points and immediately perfused with PBS. Lung-infiltrating lymphocytes were isolated using mechanical disruption of the organ. For isolation of myeloid and stromal cells from the lung, the tissue was cut into small pieces, transferred into a 24-well dish filled with RPMI 1640 medium containing 2% FCS, 20 mM Hepes pH 7.2 (all from Lonza), 1 mg/ml Collagenase Type P (Sigma-Aldrich), 25 μg/ml DNaseI (AppliChem) and 1 mg/ml Collagenase Type II (Sigma-Aldrich) in combination with gentleMACS-based mechanical disruption (Miltenyi Biotech). After 30 minutes incubation at 37°C, cell suspensions were washed with PBS containing 0.5% FCS and 10 mmol/L EDTA. Stromal cell fraction enrichment was achieved by depleting hematopoietic and erythroid cells using MACS anti-CD45 and anti-Ter119 microbeads (Miltenyi Biotec).

Cell lines

The murine B16 melanoma LacZ-expressing cell line (B16-LacZ) was obtained from RIKEN BRC (Japan) Cell No. RCB1284. Cells were cultured in Dulbecco's Modified Eagle's - Medium DMEM (low glucose) supplemented with 10% (vol/vol) FBS (Sigma-Aldrich), 100 U/mL penicillin/streptomycin (Lonza). 5×10^5 B16/LacZ cells were injected

intravenously, lungs were collected 19 days after tumor cell inoculation, lobes were separated and tumor nodules were quantified on the both sides of each lobule.

Human subjects and human cell isolation

Patient samples were obtained from the Children's Hospital and the Institute of Pathology at the Kantonsspital St. Gallen upon receiving informed consent from patients and/or their guardians. The study has been approved by the ethics committee of Eastern Switzerland as EKOS 18/113 (Assessment of target cell tropism of viral vectors in tonsillar explants), the St. Gallen Lung Biopsy Biobank (EKSG 11/044) and within the frame of the general consent at the Kantonsspital St. Gallen. The first sample was acquired on 13.11.2017, and the last sample was processed on 01.04.2019.

Tonsillar material was collected from healthy male and female children age between 3 and 14 years that are undergoing routine tonsillectomy. Inform consent signed by at least one parent or the legal guardian for children from 3 – 13 years of age, for 14-year-old children, the child also signed the informed consent. Subjects presenting the following features have been excluded from the study: 1) Major craniofacial abnormalities, 2) Undergoing immunosuppression or antibiotic treatment, 3) Major inflammatory lesions on the tonsils, 4) Patients with the pre-existing immunocompromising disease. Healthy volunteers (age 25-35) donated blood. Lung tissue obtained from a non-small cell lung cancer patient (male) undergoing debulking surgery of lung cancer and adjacent unaffected lung tissue has been obtained for the analysis. Skin tissue was obtained by a healthy patient undergoing reduction mammaplasty (female). All adult patients have signed informed consent. Tonsillar and lung tissue was mechanically disaggregated, and single-cell suspensions were generated by using the gentleMACS technique (Miltenyi Biotech). Skin cells were isolated using the MACS Whole Skin Digestion kit (Miltenyi Biotech). For in vitro culturing of human stromal cells, samples were depleted of leukocytes using anti-CD45 (Miltenyi Biotech) to enrich for stromal cell fractions. Sorted cells were assessed for viability by using trypan blue exclusion and cultured in RPMI 1640 with 5% (vol/vol) FBS (Sigma-Aldrich), 100 U/mL penicillin/streptomycin (Lonza) and 16 μg/ml gentamycin. Peripheral blood mononuclear cells (PBMCs) from healthy volunteers were isolated using a Ficoll-Paque gradient centrifugation. For in vitro infection, the cells were seeded at density of 10^6 per well in 48 well format, rested for 1 h on 37°C and infected with ChAdOx1-GFP or HuAd5-GFP using MOI of 10, 100 and 1,000. The infection was allowed for 3 h after which the medium was replaced. The cells were kept on 37°C overnight and analyzed the next day using flow cytometry.

Short-term culture of primary cells

Tonsillar tissue was extensively washed using PBS with 16 μg/ml gentamycin. The tissue was cleaned from coagulated blood, cauterized and necrotic areas, and cut into pieces size 1 x 2 x 1 mm, each containing approximately 10^6 cells [58]. During all steps the tissue was maintained in RPMI 1640 15% (vol/vol) FBS (Sigma-Aldrich), 1% (vol/vol) MEM-nonessential amino acids (Gibco), 1% (vol/vol) of MEM–sodium pyruvate (Gibco) and 16 μg/ml gentamycin. Medium-soaked Gelfoam (Pfizer) was used to ensure equally distributed nutrient availability in 1 x 1 cm pieces. Each well of a 6-well plate was filled with 3 ml of

medium and one gelfoam piece was deposited per well. Four tonsillar pieces were distributed per gelfoam piece in each well. The tissue explants were infected by carefully pipetting adenovirus vectors onto the tissue using 10^9 IU in 1 – 2 μl per tissue piece (corresponding to a MOI of 1,000) or left uninfected. Infection was allowed for 24 h at 37° C after which the tissue pieces were collected and briefly washed in PBS/gentamicin before storing overnight in 4% PFA incubation at 4°C. The following day the samples were processed for confocal microscopy.

Flow cytometry

Cell characterization was performed by incubating single cells suspensions in PBS containing 0.5% FCS and 10 mM EDTA for 25 min at 4° C, using indicated antibodies (Supplementary Table 1). Antigen specific T cell were detected using PE-conjugated $bgal_{96\text{-}103}$ and APC-conjugated $bgal_{497\text{-}504}$ tetramers (NIH Reagents) after incubation of 20 min at 37° C. Ghost Dye™ Violet 510 and 7AAD (LubioScience) was used to discriminate dead cells in flow cytometric analyses. For peptide-specific cytokine production, 10^6 lung or spleen-derived lymphocytes were restimulated with $bgal_{96\text{-}103}$ peptide (DAPIYTNV) or $bgal_{497\text{-}504}$ (ICPMYARV) (Neosystem) for 2 h at 37°C. After this, brefeldin A (5 μg/ml) was added and cells were cultured for 5 h at 37°C. Cells were stimulated with PMA (50 ng/ml) and ionomycin (500 ng/ml; both purchased from Sigma-Aldrich) as positive control or left untreated as a negative control. For intracellular or intranuclear staining, restimulated cells were surface stained and fixed using Cytofix-Cytoperm (BD Biosciences) or Foxp3/ Transcription Factor Staining Buffer Set (eBioscience) for 20 min. Fixed cells were incubated at 4°C for 40 min with anti-IFN-γ and anti-TNF (eBiosciences) mAbs, diluted in permeabilization buffer (2% FCS/0.5% saponin/PBS). Alternatively, cells were incubated in permeabilization buffer containing anti-Bcl-2 (BioLegend) or anti-Ki67 (eBioscience) anti-TOM20 (Abcam) at 4°C for 30 min. MitoTracker staining was performed according to the manufacturer's instructions (Life Technologies). Samples were analyzed by flow cytometry using a FACSFortessa flow cytometer operating programs FACSDiva, FACSChorus (BD Biosciences). Data were analyzed using FlowJo software (Tree Star).

RNA isolation and quantitative RT-PCR

T cells were sorted using antibodies CD8-FITC, 7AAD (for live/dead), tetramers PE-conjugated $bgal_{96\text{-}103}$ tetramer (NIH Reagents), and gating strategies as in Extended Data Fig. 2d. FSCs were sorted using antibodies CD45-, CD31-, EpCAM- and Ter119- PeCy7, CD34-APC, Sca-1 APC-Cy7 and 7AAD for live/dead distinction (Supplementary Table 1) and gating strategy as in Extended Data Fig. 5a and Extended Data Fig. 6d. RNA from was isolated using the Quick-RNA Mini-Prep (Zymo Research). Contaminating DNA was eliminated through on-column DNase digestion (Zymo Research). cDNA was generated using Quantitect Reverse Transcription Kit (Qiagen, USA) and quantitative RT-PCR was performed with the Light Cycler 480 SYBR Green I Master mix or Light Cycler TaqMan Master on a Quant Studio 3 machine (Applied Bioscience) using the *Il33* primer (QT00135170) and LacZ primer (Ac03987581_mr and Mr03987581_mr), *Uqcrc2* (Mm00445961_m1), *Sdha* (Mm01352366_m1) and *Cox4i1* (Mm01250094_m1). Relative gene expression analysis was calculated using the ΔΔCt method. Relative expression of samples from immunized and unimmunized lung tissue was calculated by using the

comparative cycle threshold method based on normalized expression of the housekeeping gene Hprt (QT00166768). To determine absolute gene expression a negative control, containing reagents only, and serial dilutions of plasmid containing the specific LacZ sequence were included in each run to generate a standard curve. The concentrations of the plasmid dilutions were 280,000, 28,000, 2800, 280, and 28 copies per reaction. LacZ mRNA concentration in the unknown samples was calculated using the data from the standard curve. Final copy numbers were calculated per 1,000 sorted cells.

Immunohistochemistry and confocal microscopy

Murine tissue or human tonsillar tissues pieces were fixed overnight at 4°C in freshly prepared 4% paraformaldehyde (Merck Millipore) under agitation. Tissues were embedded and oriented in 4% low-melting agarose (Invitrogen) in PBS and serially sectioned with a vibratome (VT-1200; Leica). 30-120 μm-thick sections were collected and blocked in PBS containing 10% FCS, 1 mg/mL anti-Fcγ receptor (BD Biosciences) or anti-human Fc receptor (Miltenyi Biotec), and 0.1% Triton X-100 (Sigma). Tissues were incubated overnight at 4°C with the following antibodies: anti-CD31 (Thermo Fisher), anti-CD8, anti-B220 (eBioscience), anti-ACTA2 (Thermo Fisher), anti-EYFP (Takara), anti-IL-33 (R&D systems). Human tonsillar tissue explants were characterized using anti-PDPN (eBioscience) and anti-CD45 (BD Biosciences). Unconjugated antibodies were detected with the following secondary antibodies: Alexa Fluor 488-conjugated donkey anti-rabbit-IgG, Alexa Fluor 647-conjugated goat anti-rat-IgG and Alexa Fluor 594-conjugated goat anti-rat-IgG (all purchased from Jackson Immunotools). Nuclei were stained with 4′-6-diamidino-2-phenylindole dihydrochloride (Life Technologies), and sections were mounted on glass microscopy slides by using fluorescence mounting medium (Dako). Microscopy of immunofluorescent specimens was performed with a LSM-710 confocal microscope (Carl Zeiss), and microscopy data were recorded and processed with ZEN software (Zeiss). Acquired z-stacks were reconstructed, processed for noise removal and 3D-rendering in Imaris version 9 (Bitplane) software.

Quantification of GFP-expressing cell in tonsillar tissue explants

Confocal microscopy images of human tonsillar tissue explants infected with GFP-expressing Ad vectors were processed using Imaris (Bitplane). DAPI staining was utilized to identify cell nuclei belonging specifically to single GFP-expressing (infected) cells and to determine the number of infected cells per imaged area (40x objective). Object placing function in Imaris was used to label and quantify all GFP-expressing cells. GFP^+ cells were inspected for expression of PDPN- or CD45 and marked for automated quantification. The fraction of Ad infected PDPN- or CD45-expressing cells was calculated as percentage of all GFP^+ cells quantified per imaged area.

Cell sorting, library preparation and single cell RNA-seq analysis

Fluorescence activated cell sorting was used to isolate pulmonary $EYFP^+$ cells, while excluding $CD45^+$, $CD31^+$, $EPCAM^+$ and $Ter119^+$ cells based on gating strategy as in Extended Data Fig. 5a and using antibodies listed in Supplementary Table 1. Lung associated, $bgal_{96}$-tetramer binding $CD8^+$ T cells were isolated from the lungs using antibodies CD8-FITC, 7AAD (for live/dead), tetramers PE-conjugated $bgal_{96\text{-}103}$ tetramer

(NIH Reagents), and gating strategies as in Extended Data Fig. 2d. Sorted cells were run using the 10x Chromium (10x Genomics) system, and cDNA libraries were generated according to the manufacturer's recommendations (Chromium Single-Cell 3′ Reagent Kit (v2 Chemistry and v3 Chemistry). Sequencing of the libraries was performed using NextSeq 500 or NovaSeq 6000 Illumina sequencing system at the Functional Genomic Center Zürich. Initial processing and gene expression estimation were performed using CellRanger (v3.0.2) with the Ensembl GRCm38.94 release as a reference to build index files for alignments. This preprocessing resulted in UMI counts for a total of 17,415 FSCs and 10,075 T cells. The two datasets were analyzed separately, and samples were pooled from multiple replicates from at least two independent experiments (FSCs: naive Ccl19-Cre R26R-EYFP controls, two biological replicates; immunized Ccl19-Cre R26R-EYFP, two biological replicates; T cells: Lung-associated CD8 T cells isolated from Ad-LacZ/FlexON immunized Ccl19-Cre mice, two biological replicates; lung-associated CD8 T cells isolated from intranasally DT treated, Ad-LacZ/FlexON immunized Ccl19-Cre R26R-EYFP/iDTR mice, two biological replicates) with batches spanning multiple conditions and all conditions represented by multiple batches. Scater R/Bioconductor package (v1.14.1) was used for the subsequent quality control [59] which was competed in R v3.6.1 and included the removal of cells with particularly high or low number of detected genes or UMI counts (more than two median absolute deviations from the median across all cells) or a large fraction of mitochondrial genes (more than two median absolute deviations above the median across all cells) as in [53]. Moreover, cycling cells were excluded from downstream analysis based on the expression of genes *Top2a*, *Mki67*, *Cenpf* or *Pclaf*. Contaminating hematopoietic cells, endothelial cells and epithelial cells, were excluded based on the expression of *Pecam1*, *Krt18*, *Lyve1*, *Ptprc*, *Cd79a*, *Cd3e*, *Cldn5* or *Cd53*, and only cells expressing EYFP mRNA were kept for downstream analysis. After quality control and removal of contaminants, 5,356 FSCs (2,465 cells from naive Ccl19-Cre R26R-EYFP controls; 2,891 cells from immunized Ccl19-Cre R26R-EYFP samples) and 8,393 T cells (7,211 cells from PBS treated mice; 1,182 cells from DT treated mice) were retained for further processing using the Seurat package (v3.1.1) [60]. Since, the data were collected and processed in two batches, canonical correlation analysis (cca) was used to integrate data from different batches by running the following steps as implemented in Seurat: normalization of UMI counts, regression to remove the influence of UMI counts per cell and detection of highly variable genes per batch. Data integration was done using the FindIntegrationAnchors and IntegrateData functions based on the first six correlation components (CCs) for FSCs and the first nine CCs for T cells.

Extended bioinformatics analyses

Dimensional reduction and graph-based clustering were performed on the integrated data, and FSC clusters were characterized on the basis of canonical mesenchymal cell markers and unbiased marker genes. Marker genes for each FSC cluster as well as differentially expressed genes between conditions were inferred by the Wilcoxon test as implemented in the FindMarker function of Seurat [60], and top significant genes were summarized in gene signatures based on their reported function. To investigate functional differences between T cells from DT and PBS treated mice differentially expressed genes were tested for an enrichment in gene ontologies (GO) using the *enrichGO* function from the clusterProfiler R/

Europe PMC Funders Author Manuscripts

Bioconductor package (v.3.16.0) [61]. Top significant ontologies (q value < 0.05) were visualized running the *cnetplot* function. To analyse the dynamics of fibroblast differentiation, we have run velocyto.py (v.0.17.17) [40] as a tool to predict future cell states based on the ratio of unspliced to spliced reads. Briefly, loom files were generated by running *velocyto run10x* on cellranger output and used to infer spliced and unspliced assay data. RNA velocity was estimated using the *RunVelocity* function from the SeuratWrappers R package (v.0.1.0). Further, cluster similarities were calculated as Pearson correlation between clusters based on the average expression across all genes.

Statistical analyses

All statistical analyses were performed with Prism 8.4.3 (GraphPad). Unless specified otherwise, graphs depict mean ± s.e.m. Differences between two groups were evaluated using unpaired two-tailed Student's t-tests or one- or two-way analysis of variance (ANOVA). The statistical methods used are indicated in the figure legends. Exact P values are present in the source data. Results were considered statistically significant when $P < 0.05$ (*), $P < 0.01$ (**), $P < 0.001$ (***) and $P<0.0001$ (****).

Europe PMC Funders Author Manuscripts

Extended Data

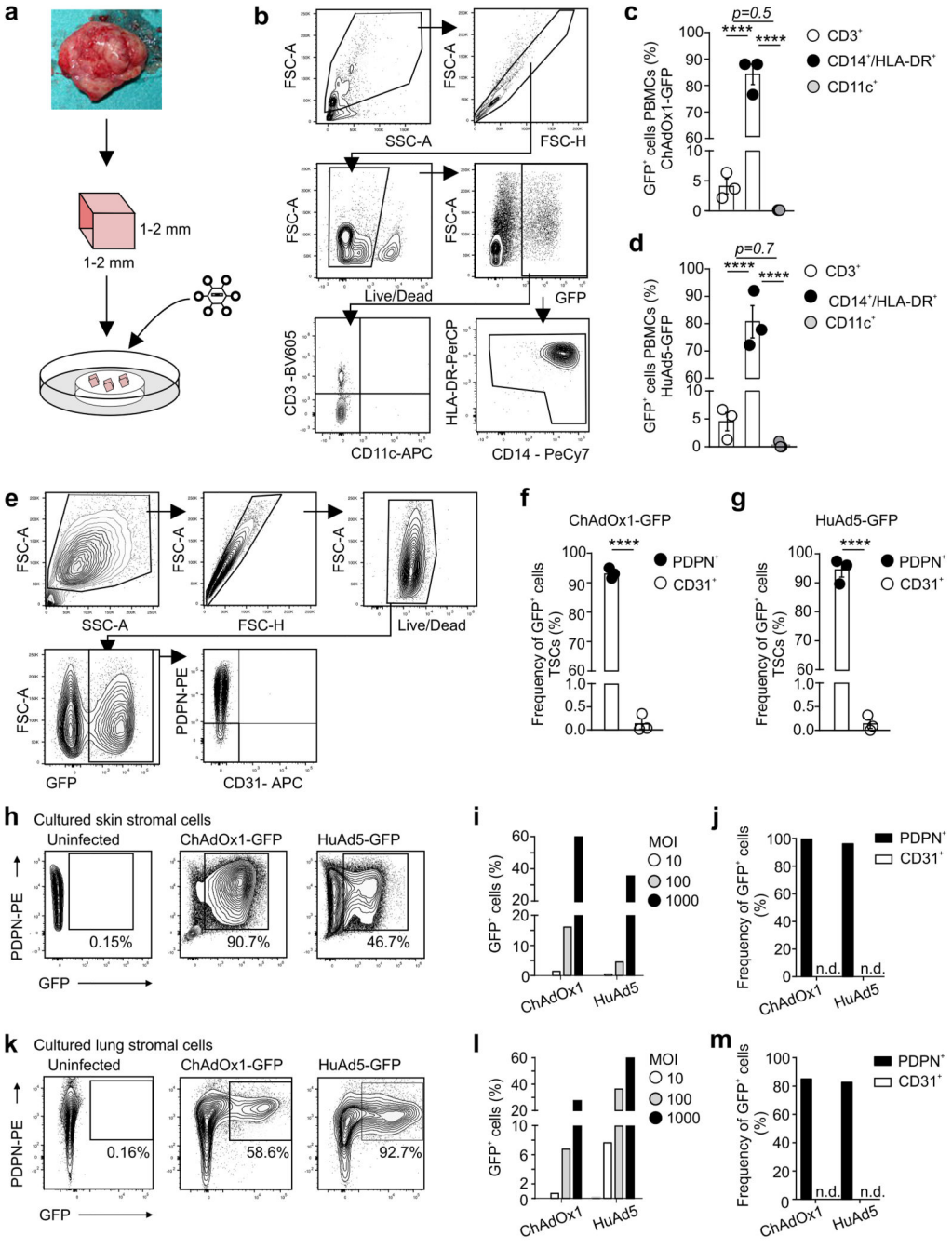

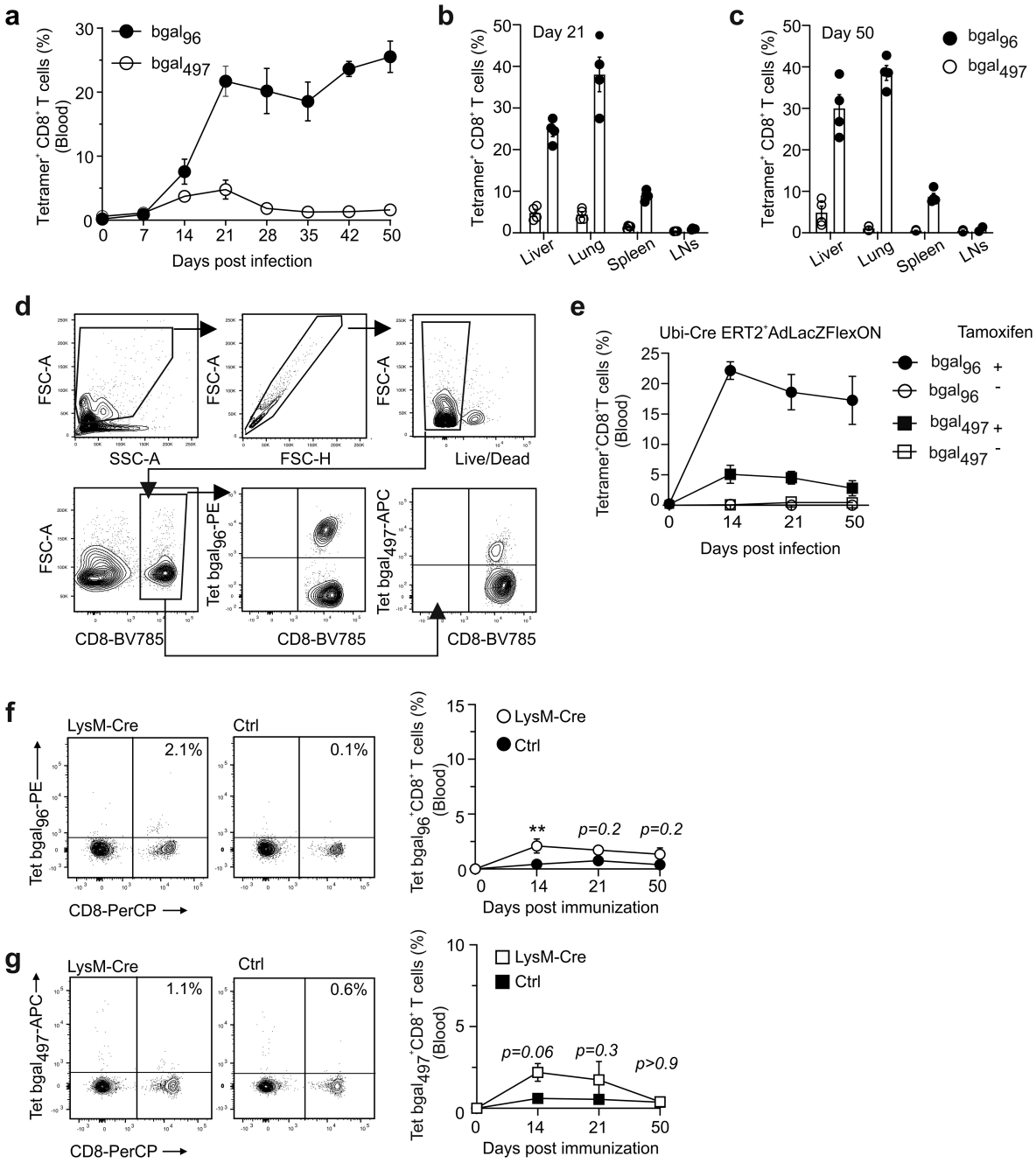

Europe PMC Funders Author Manuscripts

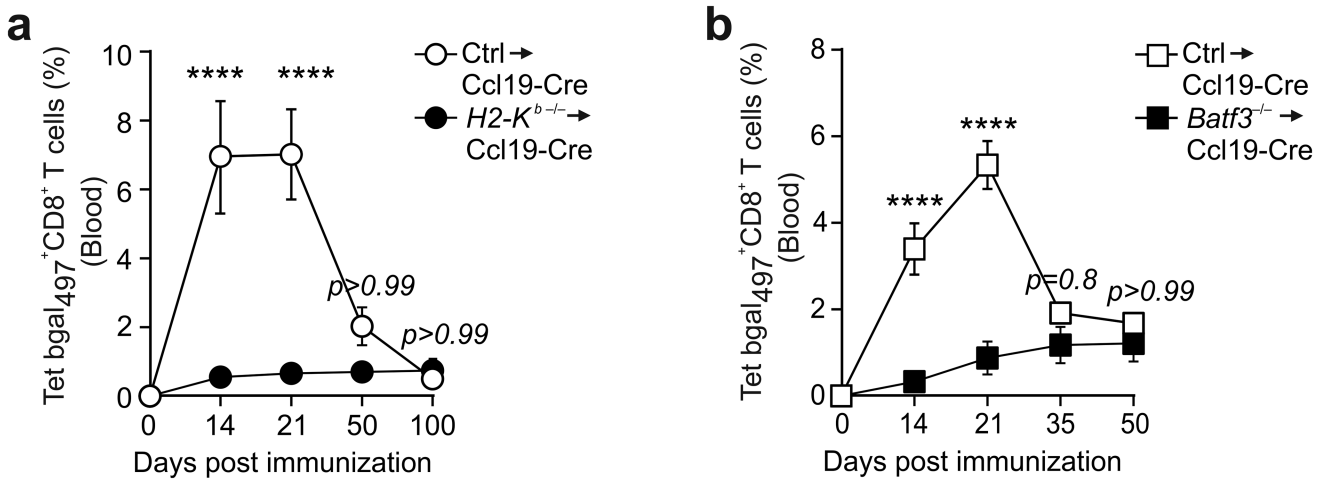

Europe PMC Funders Author Manuscripts

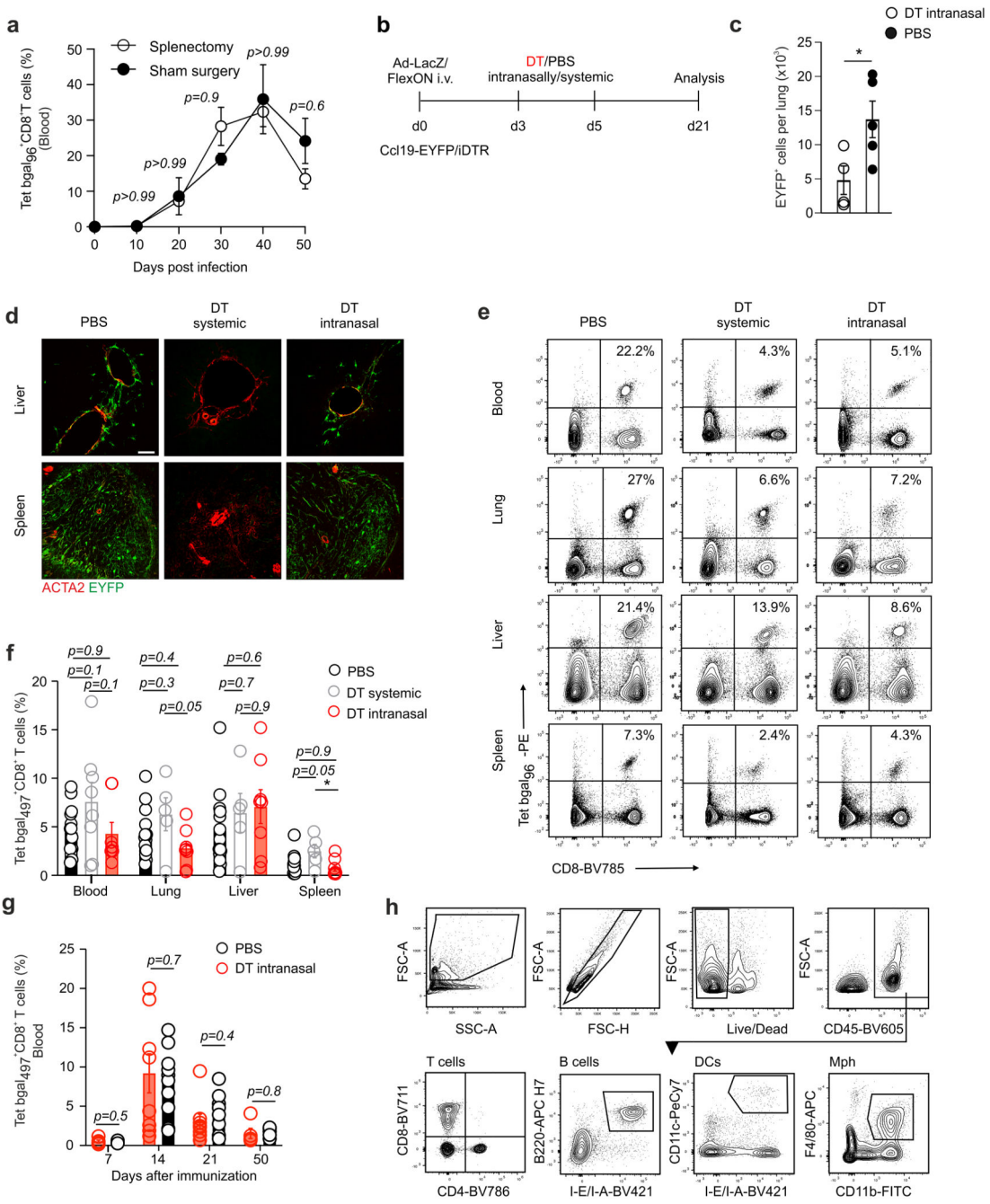

Europe PMC Funders Author Manuscripts

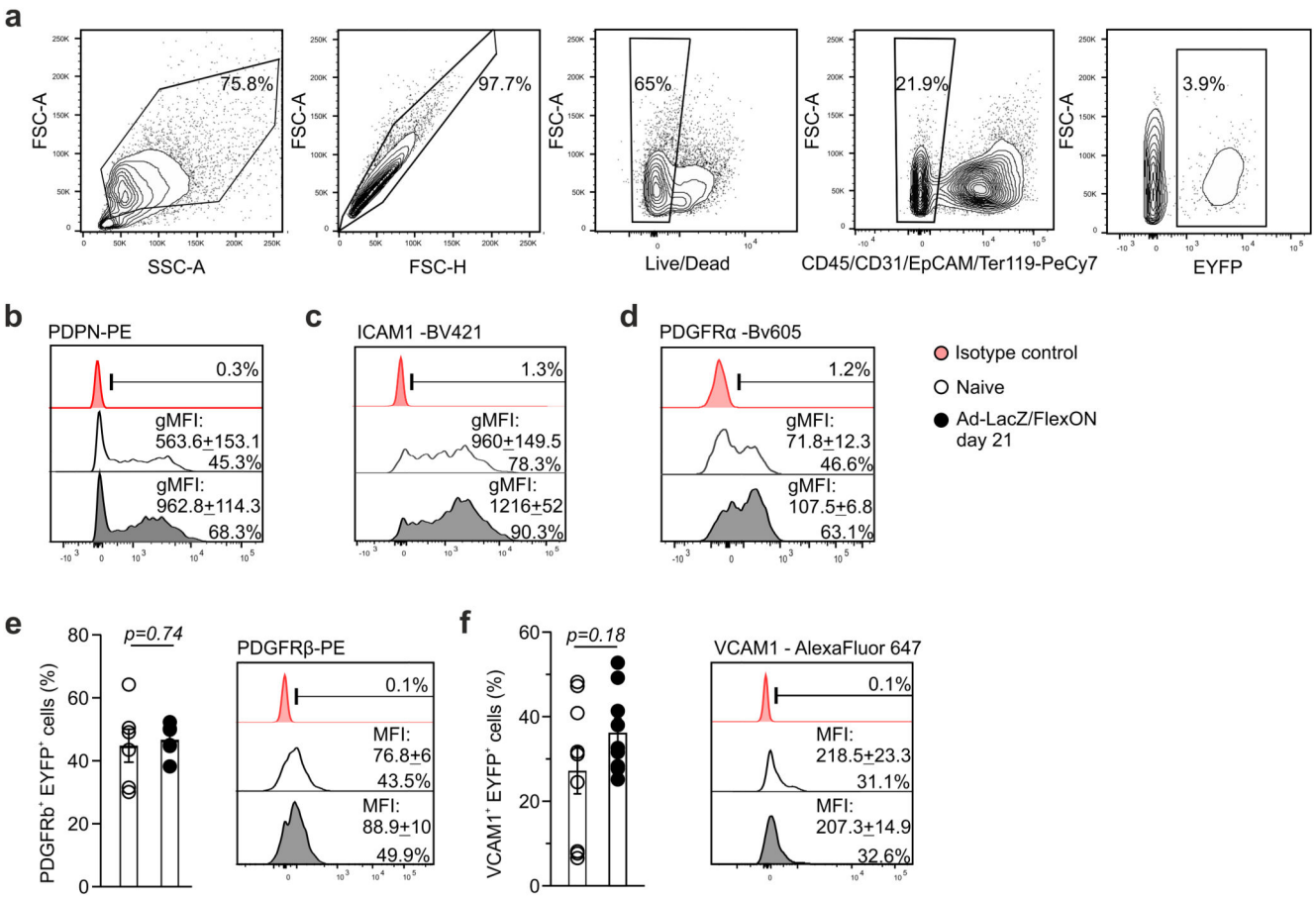

Europe PMC Funders Author Manuscripts

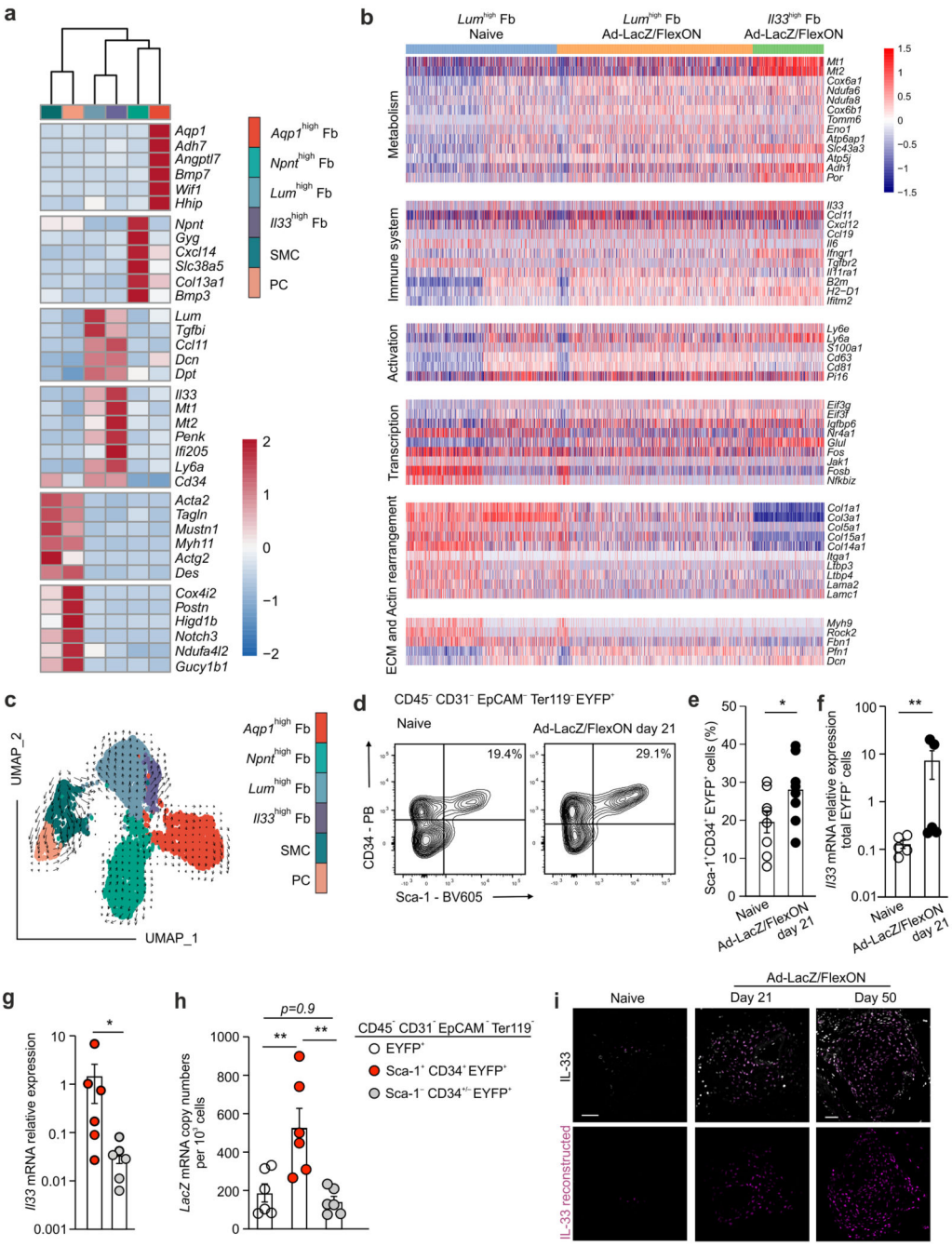

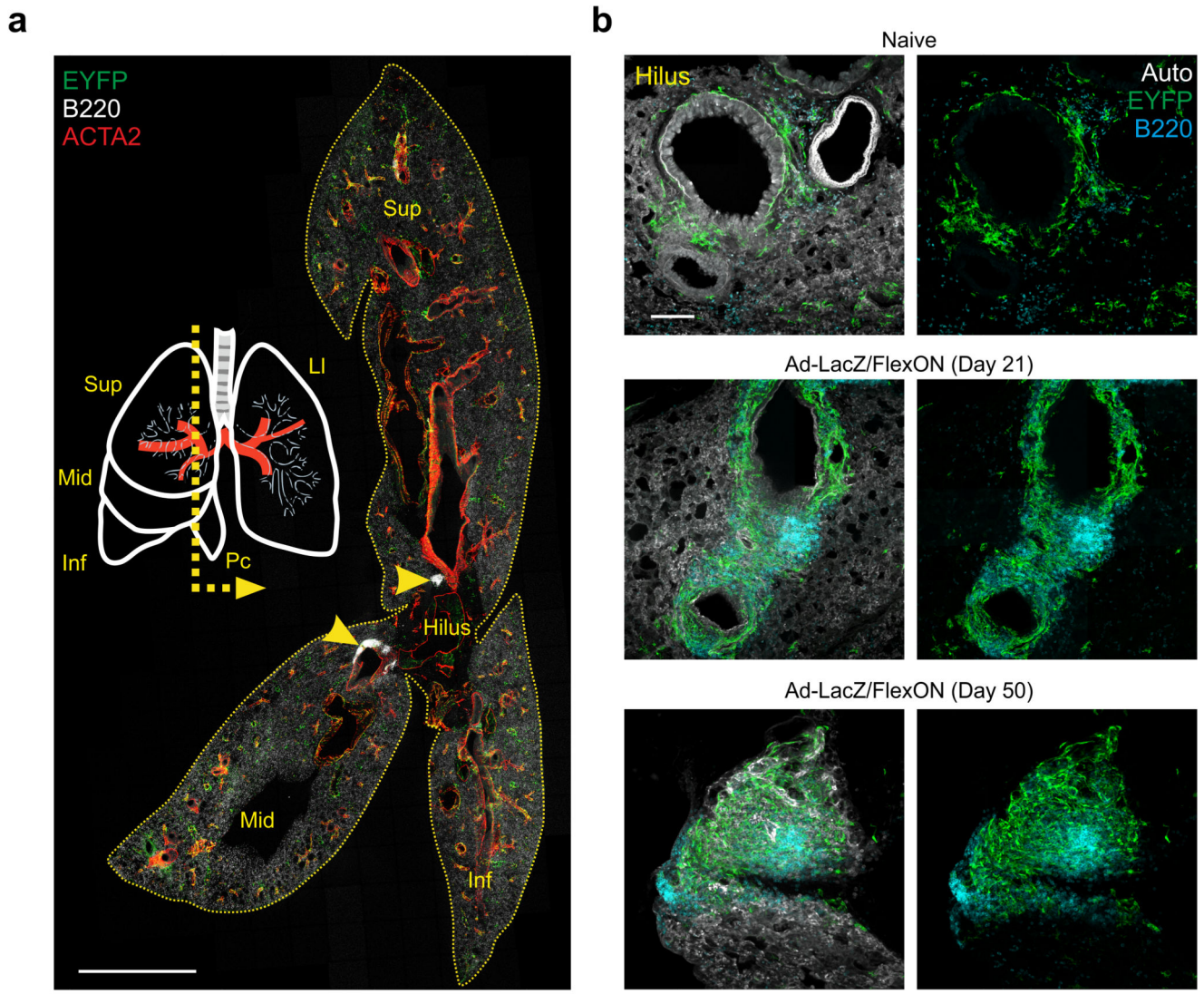

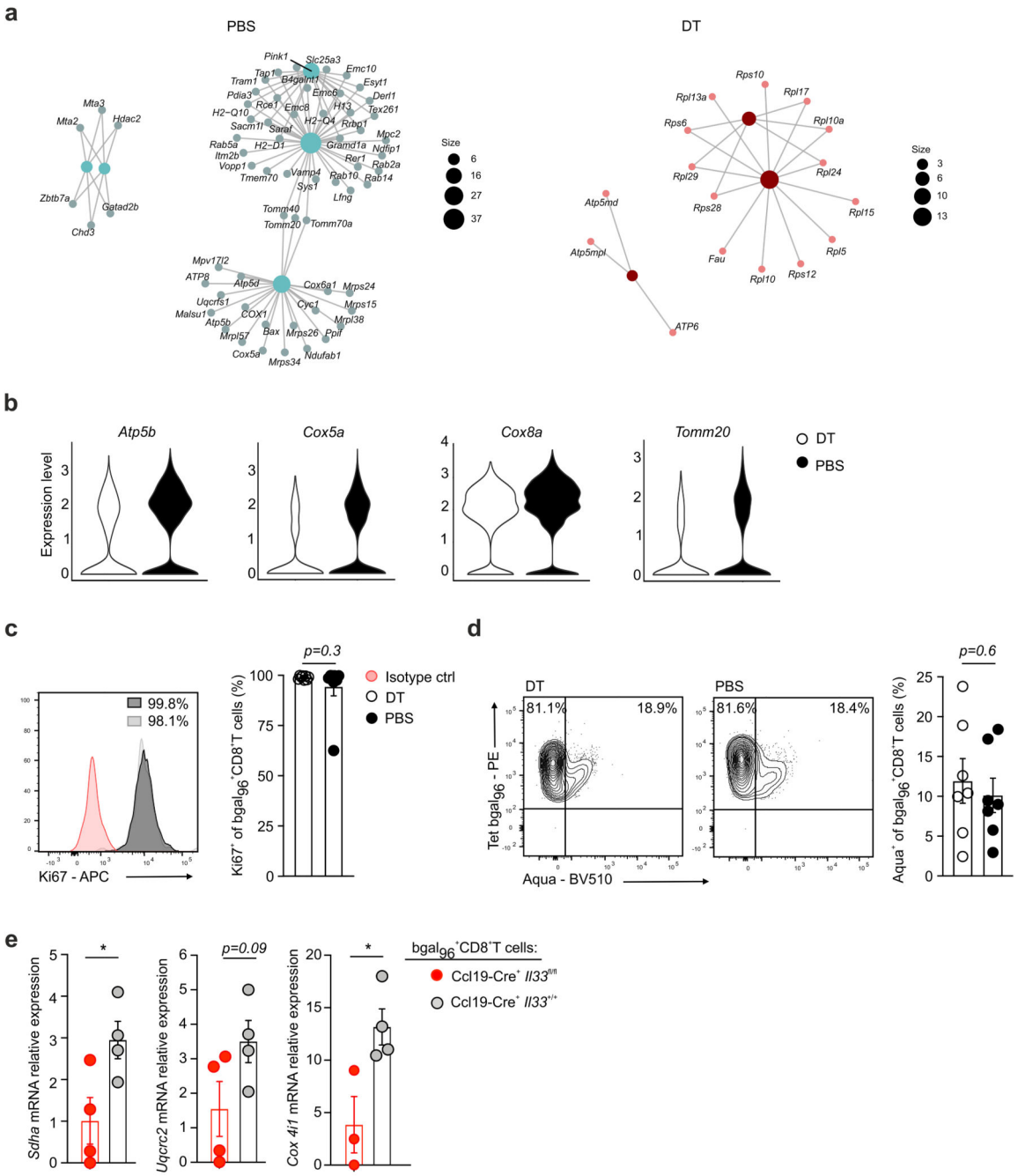

Europe PMC Funders Author Manuscripts

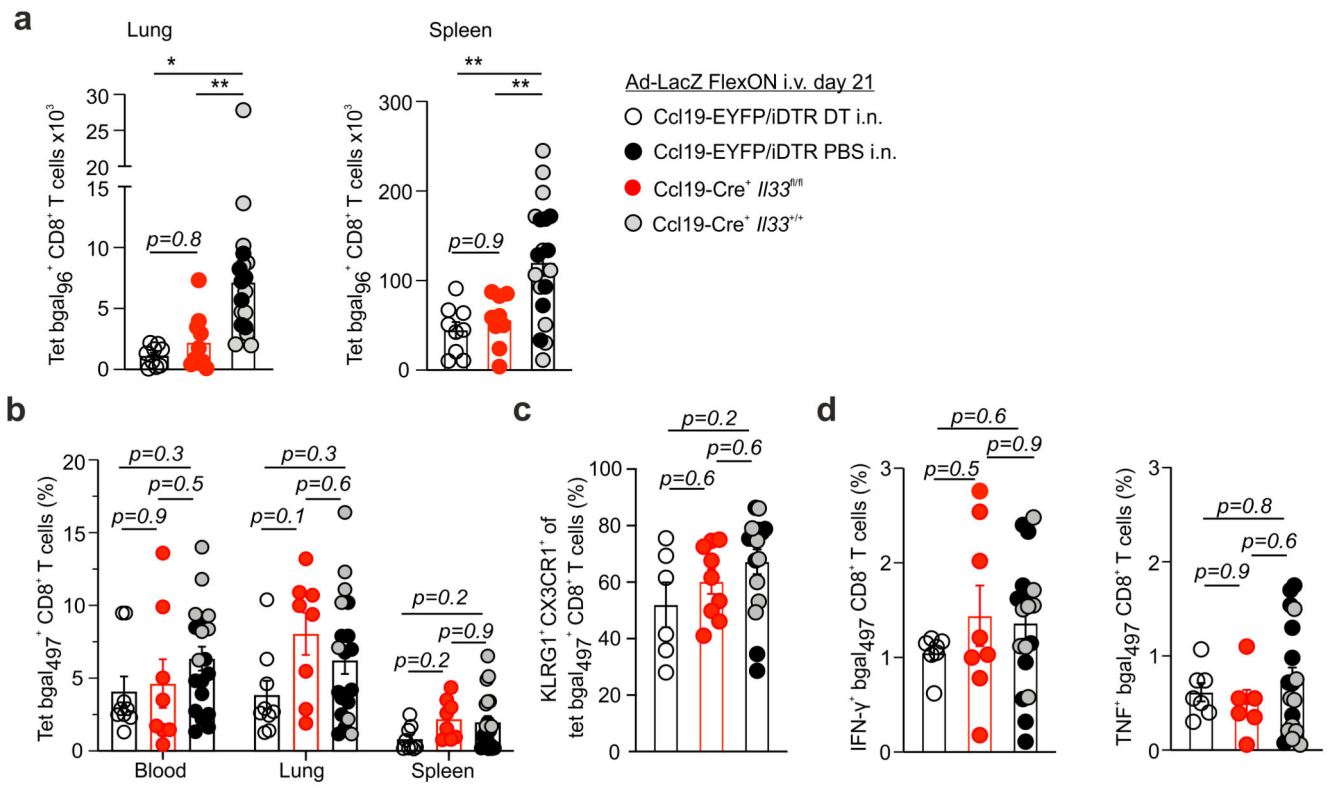

Supplementary Material

Refer to Web version on PubMed Central for supplementary material.

Acknowledgements

The authors want to thank Sonja Caviezel-Firner and Céline Engetschwiler for excellent technical support. This study received financial support from the Swiss National Science Foundation (grants 166500, 159188 to B.L.), Swiss Cancer Research (KFS-4162-02-2017-R to P.Kr.), the Wellcome Trust (109965MA to P.Kl.), and Research Fellowship Grants from the British Infection Association (to J.M.C.) and the Wellcome Trust (099897/Z/12/A to J.M.C.).

Data availability

ScRNA-seq data are available in ArrayExpress database (accession numbers E-MTAB-9558 and E-MTAB-9580). Ensembl GRCm38.94 was used as reference to build index files for alignments in scRNA-seq analysis. Further information and requests for resources should be directed to and will be fulfilled by the lead contacts, Burkhard Ludewig (burkhard.ludewig@kssg.ch) and Paul Klenerman (paul.klenerman@medawar.ox.ac.uk).

References

1. Chang JT, Wherry EJ, Goldrath AW. Molecular regulation of effector and memory T cell differentiation. Nat Immunol. 2014; 15:1104–1115. [PubMed: 25396352]

Europe PMC Funders Author Manuscripts

2. Priddy FH, et al. Safety and immunogenicity of a replication-incompetent adenovirus type 5 HIV-1 clade B gag/pol/nef vaccine in healthy adults. Clin Infect Dis. 2008; 46:1769–1781. [PubMed: 18433307]
3. Stephenson KE, et al. Immunogenicity of the Ad26.COV2.S Vaccine for COVID-19. JAMA. 2021; 325:1535–1544. [PubMed: 33704352]
4. Snook AE, et al. Split tolerance permits safe Ad5-GUCY2C-PADRE vaccine-induced T-cell responses in colon cancer patients. J Immunother Cancer. 2019; 7:104. [PubMed: 31010434]
5. Ewer K, et al. Chimpanzee adenoviral vectors as vaccines for outbreak pathogens. Hum Vaccin Immunother. 2017; 13:3020–3032. [PubMed: 29083948]
6. Folegatti PM, et al. Safety and immunogenicity of the ChAdOx1 nCoV-19 vaccine against SARS-CoV-2: a preliminary report of a phase 1/2, single-blind, randomised controlled trial. Lancet. 2020; 396:467–478. [PubMed: 32702298]
7. Ewer KJ, et al. T cell and antibody responses induced by a single dose of ChAdOx1 nCoV-19 (AZD1222) vaccine in a phase 1/2 clinical trial. Nat Med. 2021; 27:270–278. [PubMed: 33335323]
8. Barnes E, et al. Novel adenovirus-based vaccines induce broad and sustained T cell responses to HCV in man. Sci Transl Med. 2012; 4 115ra111
9. Logunov DY, et al. Safety and efficacy of an rAd26 and rAd5 vector-based heterologous prime-boost COVID-19 vaccine: an interim analysis of a randomised controlled phase 3 trial in Russia. Lancet. 2021; 397:671–681. [PubMed: 33545094]
10. Klenerman P. The (gradual) rise of memory inflation. Immunol Rev. 2018; 283:99–112. [PubMed: 29664577]
11. Karrer U, et al. Memory inflation: continuous accumulation of antiviral CD8+ T cells over time. J Immunol. 2003; 170:2022–2029. [PubMed: 12574372]
12. Sierro S, Rothkopf R, Klenerman P. Evolution of diverse antiviral CD8+ T cell populations after murine cytomegalovirus infection. Eur J Immunol. 2005; 35:1113–1123. [PubMed: 15756645]
13. Holtappels R, Pahl-Seibert MF, Thomas D, Reddehase MJ. Enrichment of immediate-early 1 (m123/pp89) peptide-specific CD8 T cells in a pulmonary CD62L(lo) memory-effector cell pool during latent murine cytomegalovirus infection of the lungs. J Virol. 2000; 74:11495–11503. [PubMed: 11090146]
14. Grzimek NK, Dreis D, Schmalz S, Reddehase MJ. Random, asynchronous, and asymmetric transcriptional activity of enhancer-flanking major immediate-early genes ie1/3 and ie2 during murine cytomegalovirus latency in the lungs. J Virol. 2001; 75:2692–2705. [PubMed: 11222693]
15. Snyder CM, et al. Memory inflation during chronic viral infection is maintained by continuous production of short-lived, functional T cells. Immunity. 2008; 29:650–659. [PubMed: 18957267]
16. Komatsu H, Sierro SAVC, Klenerman P. Population analysis of antiviral T cell responses using MHC class I-peptide tetramers. Clin Exp Immunol. 2003; 134:9–12. [PubMed: 12974748]
17. Klenerman P, Oxenius A. T cell responses to cytomegalovirus. Nat Rev Immunol. 2016; 16:367–377. [PubMed: 27108521]
18. Bolinger B, et al. A new model for CD8+ T cell memory inflation based upon a recombinant adenoviral vector. J Immunol. 2013; 190:4162–4174. [PubMed: 23509359]
19. Lee LN, et al. Adenoviral vaccine induction of CD8+ T cell memory inflation: Impact of co-infection and infection order. PLoS Pathog. 2017; 13 e1006782 [PubMed: 29281733]
20. Bassett JD, et al. CD8+ T-cell expansion and maintenance after recombinant adenovirus immunization rely upon cooperation between hematopoietic and nonhematopoietic antigen-presenting cells. Blood. 2011; 117:1146–1155. [PubMed: 21088134]
21. Krishnamurty AT, Turley SJ. Lymph node stromal cells: cartographers of the immune system. Nat Immunol. 2020; 21:369–380. [PubMed: 32205888]
22. Perez-Shibayama C, Gil-Cruz C, Ludewig B. Fibroblastic reticular cells at the nexus of innate and adaptive immune responses. Immunol Rev. 2019; 289:31–41. [PubMed: 30977192]
23. Pikor NB, Cheng HW, Onder L, Ludewig B. Development and Immunological Function of Lymph Node Stromal Cells. J Immunol. 2021; 206:257–263. [PubMed: 33397739]

24. Torti N, Walton SM, Murphy KM, Oxenius A. Batf3 transcription factordependent DC subsets in murine CMV infection: differential impact on T-cell priming and memory inflation. Eur J Immunol. 2011; 41:2612–2618. [PubMed: 21604258]
25. Torti N, Walton SM, Brocker T, Rülicke T, Oxenius A. Non-hematopoietic cells in lymph nodes drive memory CD8 T cell inflation during murine cytomegalovirus infection. PLoS Pathog. 2011; 7 e1002313 [PubMed: 22046127]
26. Busche A, et al. Priming of CD8+ T cells against cytomegalovirus-encoded antigens is dominated by cross-presentation. J Immunol. 2013; 190:2767–2777. [PubMed: 23390296]
27. Baumann NS, et al. Tissue maintenance of CMV-specific inflationary memory T cells by IL-15. PLoS Pathog. 2018; 14 e1006993 [PubMed: 29652930]
28. Rowe WP. Studies on pathogenesis and immunity in lymphocityc choriomeningitis infection of the mouse. Navy Research Report. 1954; 12:167–220.
29. Atasoy D, Aponte Y, Su HH, Sternson SM. A FLEX switch targets Channelrhodopsin-2 to multiple cell types for imaging and long-range circuit mapping. J Neurosci. 2008; 28:7025–7030. [PubMed: 18614669]
30. Chai Q, et al. Maturation of Lymph Node Fibroblastic Reticular Cells from Myofibroblastic Precursors Is Critical for Antiviral Immunity. Immunity. 2013; 38:1013–1024. [PubMed: 23623380]
31. Cheng HW, et al. Origin and differentiation trajectories of fibroblastic reticular cells in the splenic white pulp. Nat Commun. 2019; 10:1739. [PubMed: 30988302]
32. Cupovic J, et al. Central Nervous System Stromal Cells Control Local CD8(+) T Cell Responses during Virus-Induced Neuroinflammation. Immunity. 2016; 44:622–633. [PubMed: 26921107]
33. Cheng HW, et al. CCL19-producing fibroblastic stromal cells restrain lung carcinoma growth by promoting local antitumor T-cell responses. J Allergy Clin Immunol. 2018; 142:1257–1271. e4 [PubMed: 29391257]
34. Hildner K, et al. Batf3 deficiency reveals a critical role for CD8alpha+ dendritic cells in cytotoxic T cell immunity. Science. 2008; 322:1097–1100. [PubMed: 19008445]
35. Krebs P, Scandella E, Odermatt B, Ludewig B. Rapid functional exhaustion and deletion of CTL following immunization with recombinant adenovirus. J Immunol. 2005; 174:4559–4566. [PubMed: 15814677]
36. Novkovic M, et al. Topological Small-World Organization of the Fibroblastic Reticular Cell Network Determines Lymph Node Functionality. PLoS Biol. 2016; 14 e1002515 [PubMed: 27415420]
37. Zepp JA, et al. Distinct Mesenchymal Lineages and Niches Promote Epithelial Self Renewal and Myofibrogenesis in the Lung. Cell. 2017; 170:1134–1148. e1110 [PubMed: 28886382]
38. Xie T, et al. Single-Cell Deconvolution of Fibroblast Heterogeneity in Mouse Pulmonary Fibrosis. Cell Rep. 2018; 22:3625–3640. [PubMed: 29590628]
39. Tsukui T, et al. Collagen-producing lung cell atlas identifies multiple subsets with distinct localization and relevance to fibrosis. Nat Commun. 2020; 11:1920. [PubMed: 32317643]
40. La Manno G, et al. RNA velocity of single cells. Nature. 2018; 560:494–498. [PubMed: 30089906]
41. van der Windt GJ, et al. Mitochondrial respiratory capacity is a critical regulator of CD8+ T cell memory development. Immunity. 2012; 36:68–78. [PubMed: 22206904]
42. van der Windt GJ, et al. CD8 memory T cells have a bioenergetic advantage that underlies their rapid recall ability. Proc Natl Acad Sci U S A. 2013; 110:14336–14341. [PubMed: 23940348]
43. Rego GNA, et al. Current Clinical Trials Protocols and the Global Effort for Immunization against SARS-CoV-2. Vaccines (Basel). 2020; 8:474.
44. Mercado NB, et al. Single-shot Ad26 vaccine protects against SARS-CoV-2 in rhesus macaques. Nature. 2020; 586:583–588. [PubMed: 32731257]
45. Bolinger B, et al. Adenoviral Vector Vaccination Induces a Conserved Program of CD8(+) T Cell Memory Differentiation in Mouse and Man. Cell Rep. 2015; 13:1578–1588. [PubMed: 26586434]
46. Gordon CL, et al. Induction and Maintenance of CX3CR1-Intermediate Peripheral Memory CD8(+) T Cells by Persistent Viruses and Vaccines. Cell Rep. 2018; 23:768–782. [PubMed: 29669283]

47. Cohen ES, et al. Oxidation of the alarmin IL-33 regulates ST2-dependent inflammation. Nat Commun. 2015; 6:8327. [PubMed: 26365875]
48. Mager LF, et al. IL-33 signaling contributes to the pathogenesis of myeloproliferative neoplasms. J Clin Invest. 2015; 125:2579–2591. [PubMed: 26011644]
49. Dominguez D, et al. Exogenous IL-33 Restores Dendritic Cell Activation and Maturation in Established Cancer. J Immunol. 2017; 198:1365–1375. [PubMed: 28011934]
50. Bonilla WV, et al. The alarmin interleukin-33 drives protective antiviral $CD8^{+}$T cell responses. Science. 2012; 335:984–989. [PubMed: 22323740]
51. Baumann C, et al. Memory CD8(+) T Cell Protection From Viral Reinfection Depends on Interleukin-33 Alarmin Signals. Front Immunol. 2019; 10:1833. [PubMed: 31447845]
52. McLaren JE, et al. IL-33 Augments Virus-Specific Memory T Cell Inflation and Potentiates the Efficacy of an Attenuated Cytomegalovirus-Based Vaccine. J Immunol. 2019; 202:943–955. [PubMed: 30635396]
53. Pikor NB, et al. Remodeling of light and dark zone follicular dendritic cells governs germinal center responses. Nat Immunol. 2020; 21:649–659. [PubMed: 32424359]
54. Camara A, et al. Lymph Node Mesenchymal and Endothelial Stromal Cells Cooperate via the RANK-RANKL Cytokine Axis to Shape the Sinusoidal Macrophage Niche. Immunity. 2019; 50:1467–1481. e1466 [PubMed: 31201093]
55. Silva-Sanchez A, Randall TD. Role of iBALT in Respiratory Immunity. Curr Top Microbiol Immunol. 2020; 426:21–43. [PubMed: 31974759]
56. Dahlgren MW, et al. Adventitial Stromal Cells Define Group 2 Innate Lymphoid Cell Tissue Niches. Immunity. 2019; 50:707–722. e706 [PubMed: 30824323]
57. Alharbi NK, et al. ChAdOx1 and MVA based vaccine candidates against MERS-CoV elicit neutralising antibodies and cellular immune responses in mice. Vaccine. 2017; 35:3780–3788. [PubMed: 28579232]
58. Grivel JC, Margolis L. Use of human tissue explants to study human infectious agents. Nat Protoc. 2009; 4:256–269. [PubMed: 19197269]
59. McCarthy DJ, Campbell KR, Lun AT, Wills QF. Scater: pre-processing, quality control, normalization and visualization of single-cell RNA-seq data in R. Bioinformatics. 2017; 33:1179–1186. [PubMed: 28088763]
60. Stuart T, et al. Comprehensive Integration of Single-Cell Data. Cell. 2019; 177:1888–1902. e1821 [PubMed: 31178118]
61. Yu G, Wang LG, Han Y, He QY. clusterProfiler: an R package for comparing biological themes among gene clusters. OMICS. 2012; 16:284–287. [PubMed: 22455463]

Europe PMC Funders Author Manuscripts

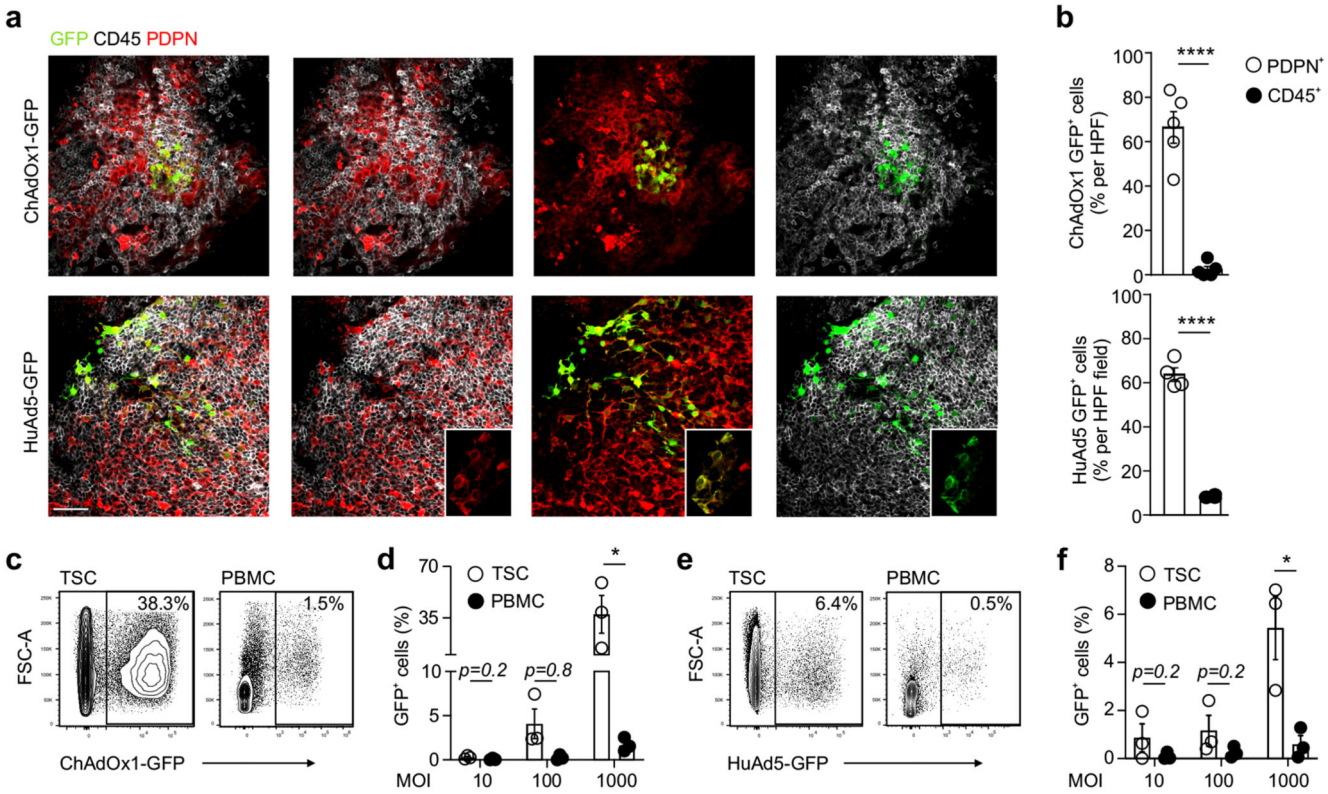

Figure 1. Adenovirus vectors target human fibroblasts.

(**a** and **b**) Infection of sliced tissue cultures from human palatine tonsils with ChAdOx1- or HuAd5-GFP. (**a**) Representative high-resolution immunofluorescence images and (**b**) frequency of GFP^+ cells within $CD45^+$ cells or $PDPN^+$ cells. Scale bar 50 μm. (**c** to **f**) Infection of cultured tissue stromal cells (TSC) or PBMCs with ChAdOx1-GFP (**c** and **d**) or HuAd5-GFP (**e** and **f**) at different MOI. (**d** and **f**) Frequency of GFP^+ cells. Dots represent individual samples and lines indicate mean ±s.e.m. Pooled data from 4 independent experiments with n=5 ChAdOx1-GFP and n=4 HuAd5-GFP tonsillar adenoid tissue samples [(b)] and 3 independent experiments with n=3 TSC or 2 independent experiments with n=3 PBMC samples [(d) to (f)]. Statistical analysis was performed using unpaired two-tailored Student's t test [(b)], [(d) and (f)] with *P < 0.05; **P < 0.01; ***P < 0.001; ****p<0.0001. Exact P values are provided in the Source Data.

Europe PMC Funders Author Manuscripts

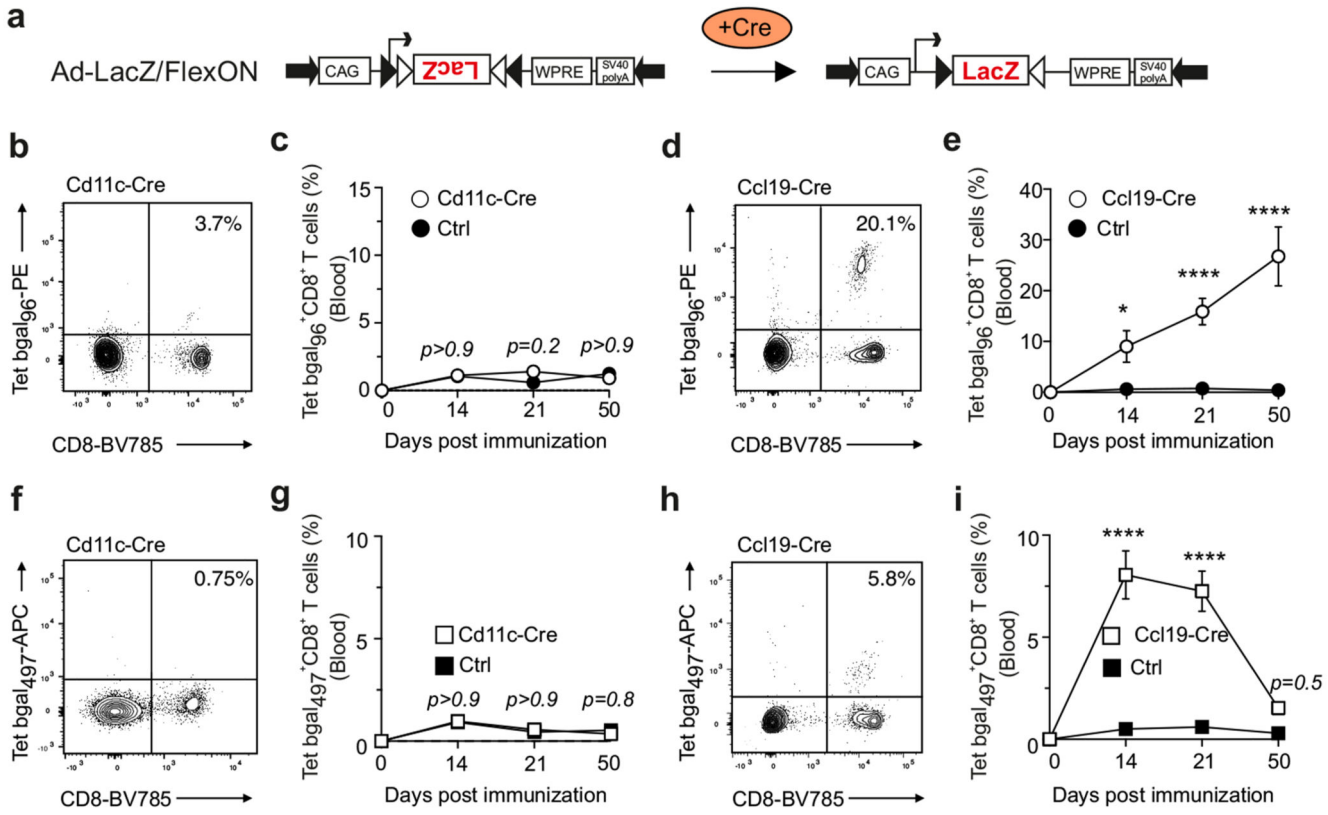

Figure 2. Ccl19-Cre-positive fibroblastic stromal cells mediate induction of inflationary memory CD8$^+$ T cells.

(**a**) Schematic depiction of HuAd5-based vectors containing a cassette with double-floxed Cre recombinase recognition sites with inverted orientation flanking the LacZ gene. Cell-type specific expression of Cre recombinase induces bgal antigen expression (Ad-LacZ/FlexON). (**b** to **i**) Kinetics of the frequency of bgal$_{96}$ tetramer$^+$ CD8$^+$ T cells (**b** to **e**) and bgal$_{497}$ tetramer$^+$ CD8$^+$ T cells (**f** to **i**) with representative FACS plots in Cd11c-Cre (**b** and **f**) and Ccl19-Cre mice (**d** and **h**). Cre-negative mice were used as controls (Ctrl). Values indicate mean±s.e.m. for each time point. Pooled data from 2 independent experiments with n=8 (Ctrl) and 11 (Cd11c-Cre) mice [(c) and (g)]; n=12 (Ctrl) and 12 (Ccl19-Cre) mice [(e) and (i)]. Statistical analysis was performed using two-way analysis of variance (ANOVA) with Bonferroni multiple comparison test [(c), (g), (e) and (i)] with *P < 0.05; **P < 0.01; ***P < 0.001; ****p<0.0001. Exact P values are provided in the Source Data.

Europe PMC Funders Author Manuscripts

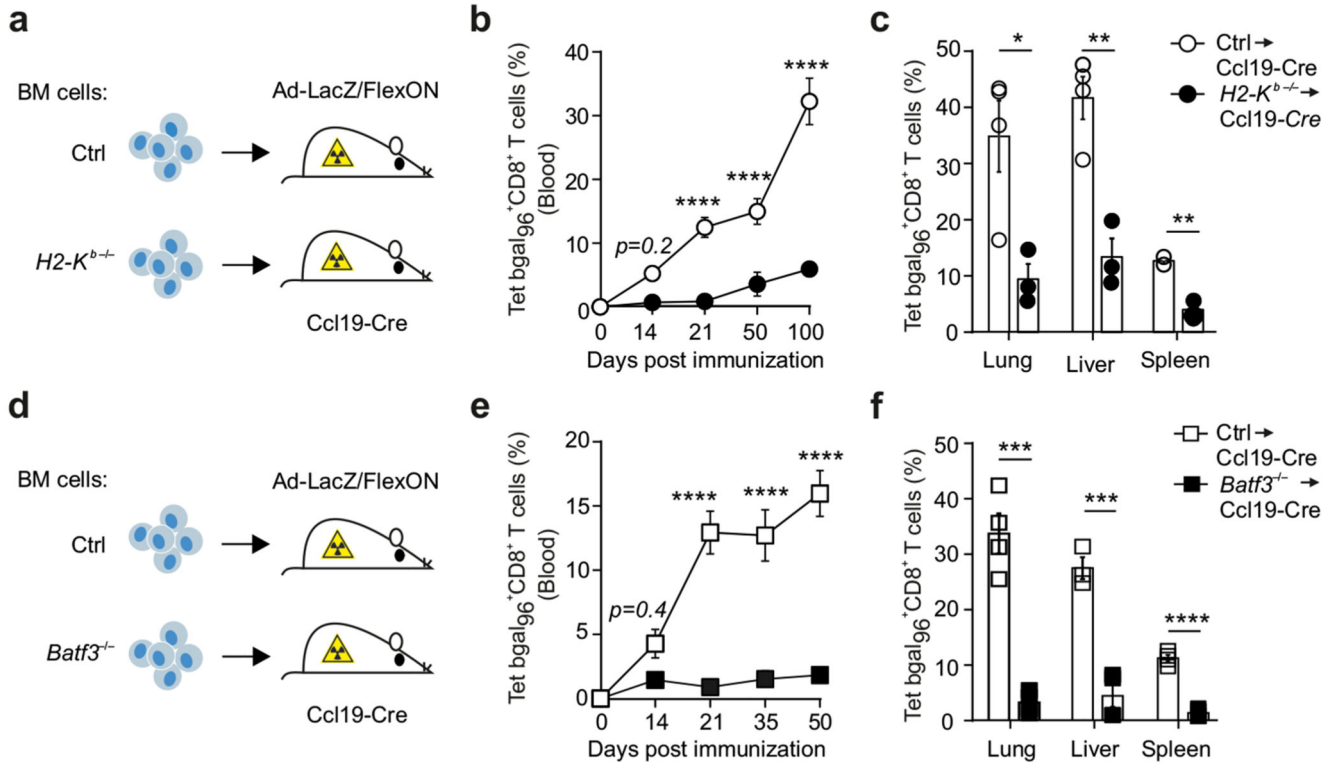

Figure 3. Ccl19-Cre^{+} FSCs collaborate with Batf3^{+} cross-presenting DCs for the induction of LacZ-specific CD8^{+} T cell responses.

Bone marrow chimeric mice were generated by transferring (**a** to **c**) *H2-K^{b}*-deficient or (**d** to **f**) *Batf3*-deficient bone marrow into sub-lethally irradiated Ccl19-Cre mice that were vaccinated i.v. with Ad-LacZ/FlexON. The frequency of bgal$_{96}$ tetramer^{+} CD8^{+} T cells was monitored in blood (**b** and **e**). On day 50, bgal$_{96}$ tetramer^{+} CD8^{+} T cells in lung, liver and spleen were analyzed (**c** and **f**). Pooled data from 2 independent experiments with n=10 (Ctrl to Ccl19-Cre) to 8 (*H2-K^{b} $^{-/-}$* to Ccl19-Cre) mice [(b)]; n= 4 (Ctrl to Ccl19-Cre) to 3 (*H2-K^{b} $^{-/-}$* to Ccl19-Cre) mice [(c)]; n=5 (Ctrl to Ccl19-Cre) and 5 (*Batf3 $^{-/-}$* to Ccl19-Cre) mice [(e)] and n=4 (Ctrl to Ccl19-Cre) and 4 (*Batf3 $^{-/-}$* to Ccl19-Cre) mice (f)]. Values indicate mean ±s.e.m. for each time point or organ analyzed. Statistical analysis was performed using two-way analysis of variance (ANOVA) with Bonferroni multiple comparison test [(b) and (e)], unpaired two-tailored Student's t test [(c) and (f)] with *P < 0.05; **P < 0.01; ***P < 0.001; ****p<0.0001. Exact P values are provided in the Source Data.

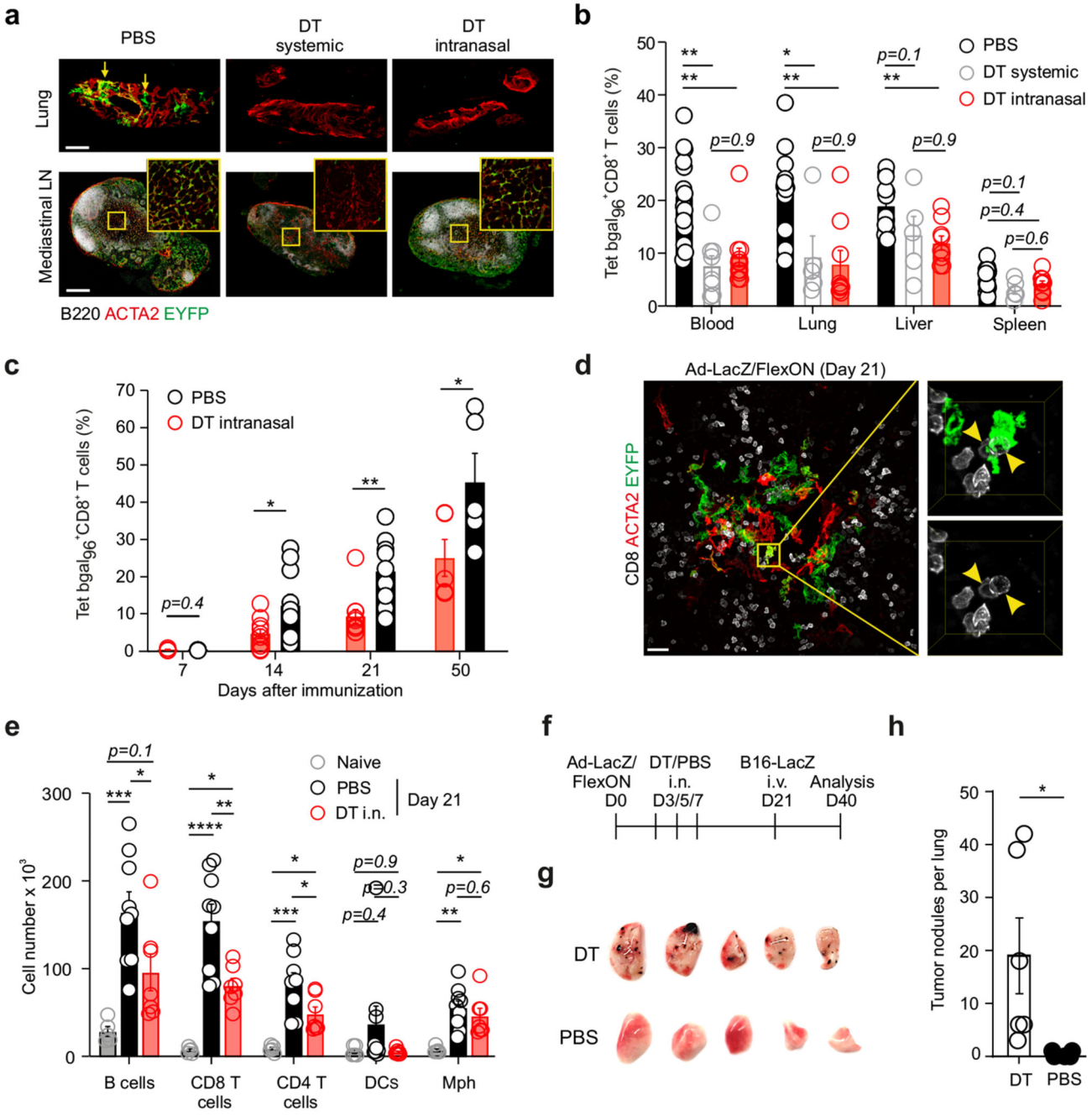

Figure 4. Pulmonary Ccl19-Cre^{+} FSCs support inflating memory CD8^{+} T cells.

(**a** to **e**) Ccl19-EYFP/iDTR mice were i.v. immunized with Ad-LacZ/FlexON and treated intranasally/systemically with diphteria toxin (DT) or PBS. (**a**) Representative confocal microscopy images of EYFP^{+} FSCs in lung and mediastinal lymph node after intranasal or systemic DT injection. Boxed and enlarged areas show the stromal network in the T cell zone of the lymph node. Scale bars 150 μm (overview) and 40 μm (boxed areas). (**b**) Frequency of bgal$_{96}$ tetramer^{+} CD8^{+} T cells in the indicated organs. (**c**) Frequency of bgal$_{96}$ tetramer^{+} CD8^{+} T cells in the blood at the indicated time points. (**d**) Representative high-

resolution immunofluorescence image of lungs from Ccl19-Cre-EYFP mice immunized i.v. with Ad-LacZ/FlexON. Arrowheads in the boxed area indicate $CD8^+$ T cells in close proximity to $EYFP^+$ FSCs. Scale bar 20 μm. (**e**) Enumeration of immune cell populations in the lungs on day 21 in Ad-LacZ/FlexON-vaccinated mice following i.n. DT or PBS application or in naive mice, gating strategy Extended data Fig. 4h. (**f**) Treatment scheme for Ccl19-Cre-EYFP/iDTR mice immunized with Ad-LacZ/FlexON and challenged i.v. with LacZ-expressing B16F10-melanoma cells. (**g** to **h**) Analysis of lungs for pulmonary tumor metastases with representative images (**g**) and quantification (**h**). Values indicate mean ±s.e.m. for each time point or organ analyzed. Pooled data from 2 independent experiments with n=3 (DT systemic), n=7 (DT intranasal) and n=5 (PBS control) mice [(a)]; n=5 (8 blood) (DT systemic), n=9 (11 blood) (DT intranasal) and n=14 (PBS control) mice [(b)]; n=5 (days 7 and 50), 10 mice (day 14) and 8 (day 21) [(c)]; n= 3 mice [(d)]; n=5 (naive), n=9 (PBS, day 21) and n=7 (DT intranasal, day 21) mice [(e)]; and n=6 mice [(g, h)]. Statistical analysis was performed using one-way ANOVA with Tukey`s multiple comparison test [(b) and (e)] and using unpaired two-tailored Student’s t test with [(c, h)]. *P < 0.05; **P < 0.01; ***P < 0.001; ****p<0.0001. Exact P values are provided in the Source Data.

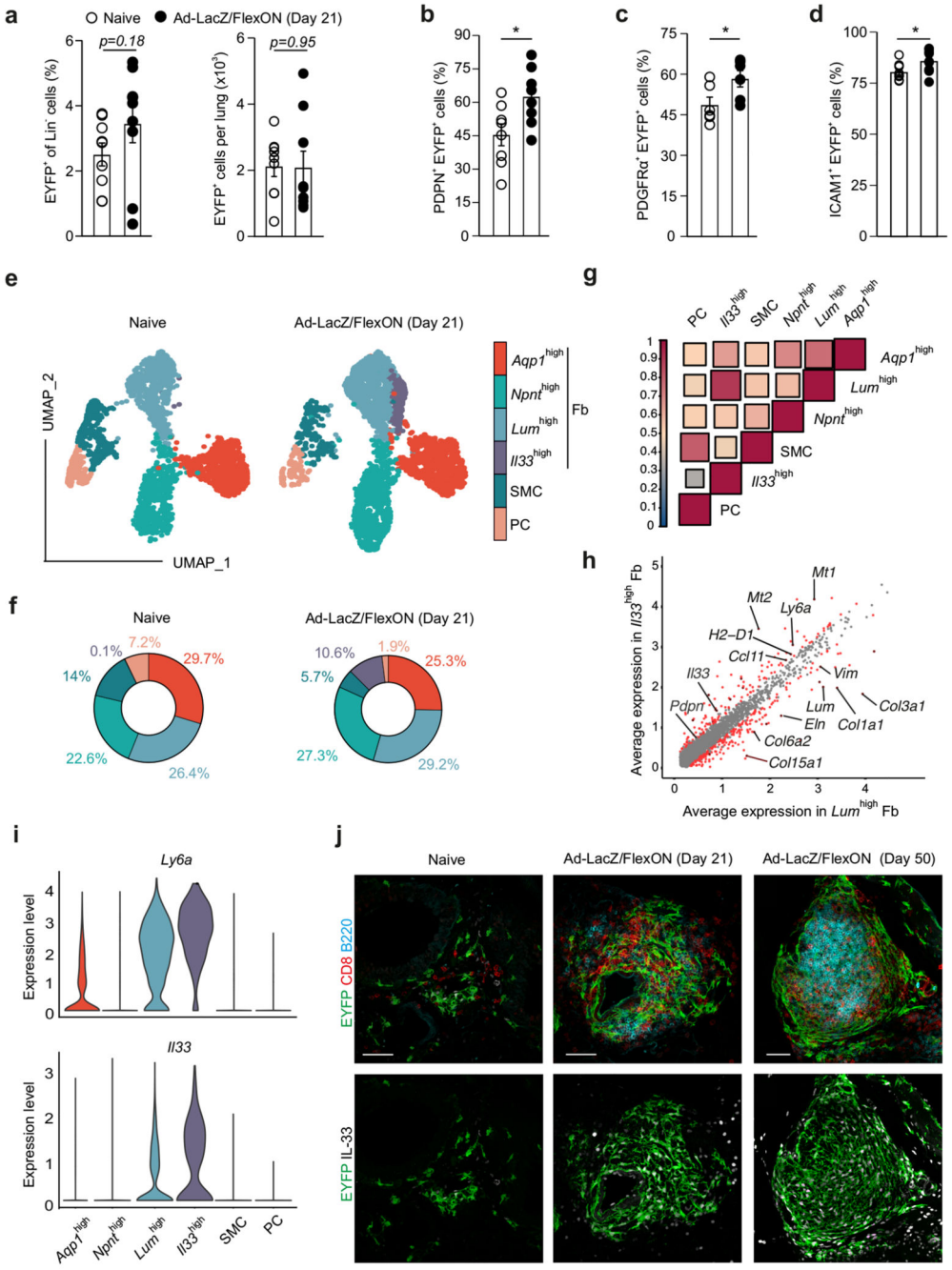

Figure 5. Ad-LacZ/FlexON activates pulmonary Ccl19-expressing, immune-stimulatory FSCs.

Ccl19-Cre EYFP mice were immunized i.v. with Ad-LacZ/FlexON and pulmonary stromal cells were analyzed on day 21. (**a**) Frequency (left panel) and absolute numbers of recovered EYFP$^+$ cells (right panel). (**b** to **d**) Frequency of PDPN$^+$ (**b**), PDGFRα$^+$ (**c**) and ICAM1$^+$ cells (**d**) within the EYFP$^+$ population. (**e** to **i**) Single cell RNA-seq analysis of EYFP$^+$ cells isolated from lungs of Ccl19-Cre EYFP mice treated i.v. with Ad-LacZ/FlexON on day 21 or naive Ccl19-Cre EYFP mice. Gating strategy Extended Data Fig. 5a. (**e**) UMAP plots indicate FSCs cluster assignment in naive control or Ad-LacZ/FlexON-treated mice. (**f**) Pie

charts displaying relative abundance of the identified pulmonary FSC clusters. (**g**) Correlation plot of $EYFP^{+}$ pulmonary FSCs depicting similarity between identified FSC clusters calculated as Pearson correlation based on the average gene expression. (**h**) Scatter plot showing average gene expression of *Il33* ^{high} FSCs vs *Lum* ^{high} FSCs in merged data from naive control and Ad-LacZ/FlexON-treated mice. (**i**) Violin plots show expression of *Il33* and *Ly6a*. (**j**) Representative confocal microscopy images of BALT formation in the lungs of immunized Ccl19-EYFP mice on days 21 and 50. Scale bars 30 μm. ScRNA-seq analysis was performed with two biological replicates for n=6 naive Ccl19-Cre EYFP mice and n=5 Ad-LacZ/FlexON-treated mice. We obtained 2,465 (naive) and 2,891 (Ad-LacZ/FlexON) EYFP-expressing cells. Dots in (a-d) represent individual mice and means±s.e.m. are shown. Pooled data from 2 independent experiments with n=9 mice [(a)]; n=8 [(b)]; n=6 [(c)]; and n=9 [(d)]. Representative images from two independent experiments, n=4 mice per group [(j)]. Statistical analysis was performed using unpaired two tailored Student's t test [(a) to (d)] with *P < 0.05: **P < 0.01; ***P < 0.001; ****p<0.0001. Exact P values are provided in the Source Data.

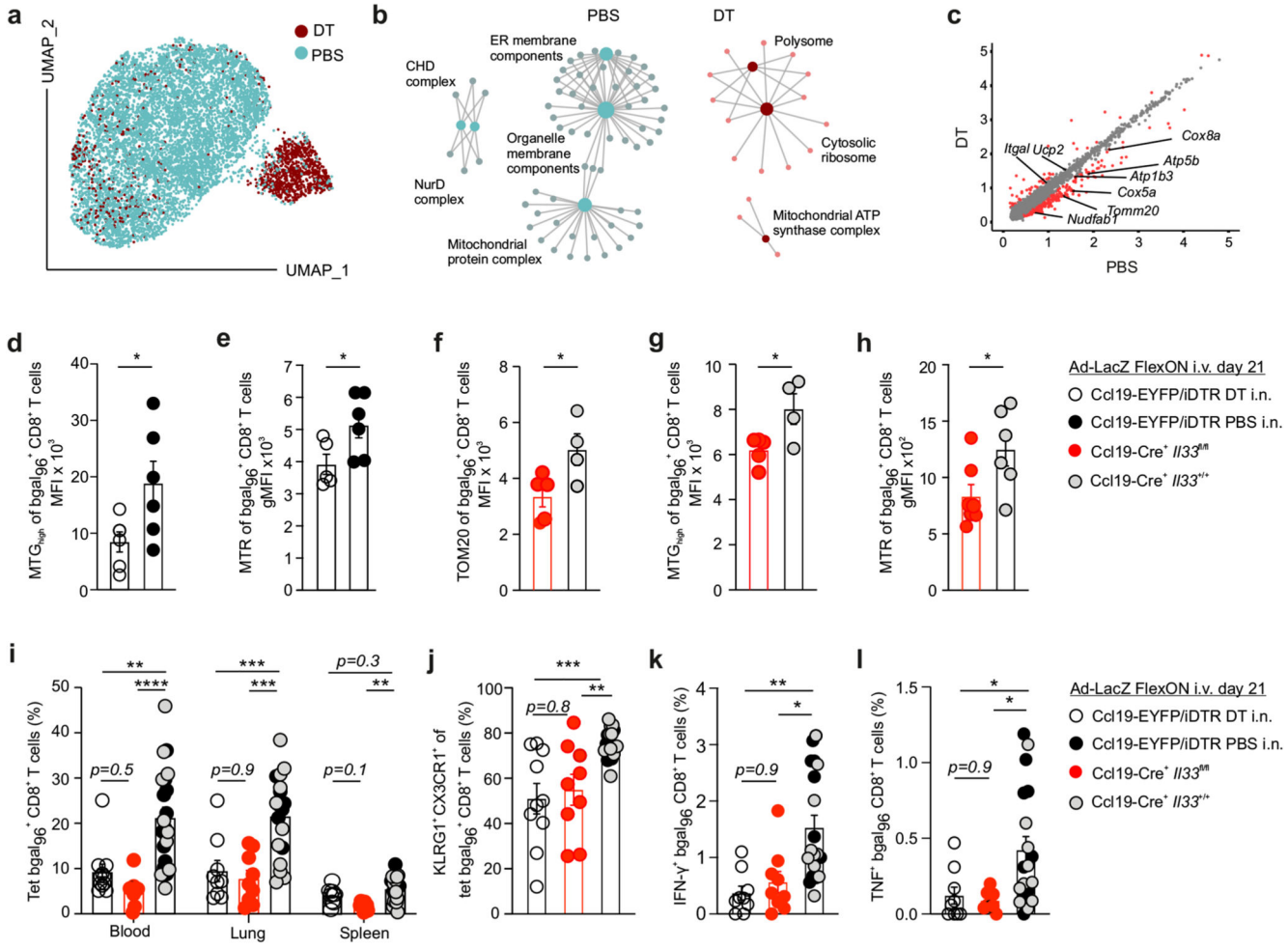

Figure 6. Pulmonary FSC-derived IL-33 preserves metabolic and functional fitness of inflationary memory CD8$^+$ T cells.

(**a** to **e**) Ccl19-Cre-EYFP/iDTR mice were immunized i.v. with Ad-LacZ/FlexON and treated with DT or PBS, days 3 and 5. Sc RNA-seq analysis of lung derived bgal$_{96}$-specific CD8$^+$ T cells (Gating strategy Extended Data Fig. 2d). (**a**) UMAP plots of bgal$_{96}$-specific CD8$^+$ T cell. (**b**) Network plots displaying most significantly enriched gene ontologies and the number of enriched genes based on transcriptional differences in bgal$_{96}$-specific CD8$^+$ T cells. (**c**) Scatter plot displaying differentially expressed genes in bgal$_{96}$-specific CD8$^+$ T cells. (**d** and **e**) Mean expression of MitoTrackerGreen in MTG-high population (MTG$_{high}$) (**d**) and geometric mean of MitoTrackerRed (MTR) (**e**) on pulmonary bgal$_{96}$-specific T cells. (**f** to **h**) Ccl19-Cre *Il33* $^{fl/fl}$ mice or Ccl19-Cre *Il33* $^{+/+}$ mice were immunized i.v. with Ad-LacZ/FlexON. Mean expression of TOM20 (**f**) MitoTrackerGreen in MTG-high fraction (MTG$_{high}$) (**g**), and geometric mean of MitoTrackerRed (MTR) (**h**) on pulmonary bgal$_{96}$-specific T cells. (**i** to **l**) CD8$^+$ T cells were analyzed 21 days after Ad-LacZ/FlexON immunization of Ccl19-Cre-EYFP/iDTR and Ccl19-Cre *Il33* $^{fl/fl}$ mice. Ccl19-Cre-EYFP/iDTR mice were treated i.n. with DT or PBS, days 3 and 5. (**i**) Frequency of bgal$_{96}$-specific T cells in blood, lung and spleen. (**j**) Frequency of KLRG1$^+$ CX3CR1$^+$ bgal$_{96}$-specific T cells in the lungs. (**k** and **l**) IFN-γ- and TNF-producing pulmonary bgal$_{96}$-specific CD8$^+$ T

cells. Dots represent individual mice. Bar graphs indicate mean and lines show±s.e.m. ScRNA-seq analysis was performed with two biological replicates for n=5 PBS- and n=6 DT-treated, Ad-LacZ/FlexON-immunized, Ccl19-Cre-EYFP/iDTR mice. Pooled data from 2 independent experiments with n=6 mice per group [(d) and (e)]; n=7 (Ccl19-Cre^{+} *Il33*$^{fl/fl}$) and n=6 Ccl19-Cre^{+} *Il33*$^{+/+}$) mice [(h)]; n=9 (DT intranasal), n=9 (Ccl19-Cre^{+} *Il33*$^{fl/fl}$) and n=18 (Ccl19-EYFP/iDTR PBS i.n. and Ccl19-Cre^{+} *Il33*$^{+/+}$) [(i)]; n=9 (DT intranasal), n=9 (Ccl19-Cre^{+} *Il33*$^{fl/fl}$) and n=19 (Ccl19-EYFP/iDTR PBS i.n. and Ccl19-Cre^{+} *Il33*$^{+/+}$) [(j), (k) and (l)] and representative of 2 independent experiments each n=5 (Ccl19-Cre^{+} *Il33*$^{fl/fl}$) and n=4 Ccl19-Cre^{+} *Il33*$^{+/+}$) mice [(f), (g)]. Statistical analysis was conducted using unpaired two-tailored Student's t test [(d) to (h)] or one-way ANOVA with Tukey`s multiple comparison test [(i) to (l)] with *P < 0.05; **P < 0.01; ***P < 0.001; ****p<0.0001. Exact P values are provided in the Source Data.